Heliyon 10 (2024) e32862

Contents lists available at ScienceDirect

Heliyon

journal homepage: www.cell.com/heliyon

Research article

Modified effective butterfly optimizer for solving optimal power flow problem

Kadir Abaci [a], Zeki Yetgin [b], Volkan Yamacli [b,*], Hakan Isiker [a]

[a] Electrical & Electronics Engineering Department, Faculty of Engineering, Mersin University, P.O. Box 33343, Mersin, Turkey
[b] Computer Engineering Department, Faculty of Engineering, Mersin University, P.O. Box 33343, Mersin, Turkey

ARTICLE INFO

Keywords:
Power system
Optimal power flow
Modified effective butterfly algorithm
Optimization

ABSTRACT

The optimal power flow (OPF) problem remains a popular and challenging work in optimizing power systems. Although researchers have suggested many optimization algorithms to solve this problem in the literature, their comparison studies lack fairness and transparency. As these studies increase in number, they deviate from a standard test system, considering a common security and technical constraints., there is a growing trend away from a standard test system. Different studies used different search ranges for the same decision and constraint parameters, different than the standard ranges suggested by IEEE systems. This caused many unfair comparisons in literature. Furthermore, these studies are generally not transparent enough so that their results cannot be verified. This has resulted in numerous infeasible solutions in the literature, violating the limits of constraint parameters. The recent incorporating of renewable energy sources in OPF studies has made this situation more complicated. Sorting through the literature and identifying those OPF applications having exactly the same test conditions is a challenging process. The main contribution is this paper adapts the modified effective butterfly algorithm (MEBO) to solve OPF problem under the common parameter constraints and sufficient transparency. The focus is on a transparent comparison with works in the literature with the same constraint values. This paper compares the performance of the proposed algorithm with other state-of-the-art algorithms in the literature, focusing on the wind energy and without wind energy IEEE 30-bus and IEEE 57-bus systems and the most commonly used constraints. The results demonstrate the efficiency and superiority of the proposed algorithm. For instance, in the 30-bus test system, compared to the initial case, fuel cost has been reduced by 11.42 %, emission by 14.33 %, L-index by 45.10 %, active power losses by 51.60 %, and voltage deviation by 92.70 %.

1. Introduction

Since the optimal power flow was first proposed by Carpentier in 1962, numerous classical and intelligence-based methods have been used to solve this problem. OPF is generally characterized as a large-scale, non-linear, non-convex, multidimensional, and numerical problem that depends on line and bus data. The complexity of OPF is further increased by including variable constraints while optimizing and satisfying the system parameters for the objective functions. By determining the active output powers and voltages of

* Corresponding author.
E-mail addresses: kabaci@mersin.edu.tr (K. Abaci), zyetgin@mersin.edu.tr (Z. Yetgin), vyamacli@mersin.edu.tr (V. Yamacli), hakan.isiker@mersin.edu.tr (H. Isiker).

https://doi.org/10.1016/j.heliyon.2024.e32862
Received 13 March 2024; Received in revised form 7 May 2024; Accepted 11 June 2024
Available online 16 June 2024

the generators, in addition to the reactive power output values of the shunt capacitor banks and the tap settings of the on-load tap changers, the optimal power flow's primary goal can be defined as optimizing a specific objective function while satisfying physical, operational, and security constraints.

At first, classical mathematic-based programming methods such as Gradient-based method for the solution of the OPF problem was the reduced gradient method, proposed by Carpentier [1]. Then, Dommel and Tinney [2] presented the formulation of optimal power flow and worked out the problem based on the Kuhn–Tucker optimality criterion using a combination of the gradient method for a known group of independent variables and penalty functions by non-linear programming, also, Quintana et al. [3,4] have demonstrated the efficacy of a penalty function in solving the reactive power dispatch problem through the use of linear programming, a technique that is both fast and reliable. However, it is important to note that this approach also has a number of inherent disadvantages. In the past, other techniques have been employed to address this problem, including quadratic programming by Burchett et al. [5] and a Newton-based method by Tinney et al. [6,7]. Also, sequential unconstrained minimization technique [8] and interior point methods (IPMs) [9] have been contributed solving of the optimal power flow problem. While these methods have also been shown to be effective in certain contexts, they also have a number of limitations. However, these methods have inherent limitations, including convexity, continuity assumptions, and a tendency to converge to local optima due to their reliance on gradient-based searches. Additionally, the OPF problem is non-linear and has multiple optimal solutions, including local and global optima. Therefore, conventional methods are not suitable for reaching the global optimum and are ill-equipped to handle non-differentiable objective functions and cost functions such as piecewise type, multiple fuel types and limitations.

Using meta-heuristic algorithms instead of classical optimization methods has become indispensable in recent years to solve the OPF problem involving multiple independent single-objective functions. In the early stages of solving OPF problems with meta-heuristic approaches, genetic algorithms, and improved genetic algorithms [10,11], conventional evolutionary programming (EP) [12] gained prominence. In the following years, new versions based on genetic algorithms such as enhanced genetic algorithm (EGA) [13], GA-fuzzy system approach (GA-FSA) [14], EGA with new decomposed quadratic load flow (EGA-DQLF) [15] and improved EP (IEP) [16] were introduced to the literature. In this area, other subsequent methods include differential evolution (DE) where the OPF problems are solved using multiple fuel options, which made some improvements [17] and its versions such as self-adaptive differential evolution by augmented Lagrange multiplier method (SADEALM) [18], modified DE (MDE) [19] that new penalty method was proposed to search for the best solution during the mutation phase. Also, hybrid differential evolution simulated annealing and tabu search based algorithm (HDE-SATS) [20] and adaptive constrained differential evolution (ACDE) [21] and effective constraint handling techniques differential evolution [22] are employed to overcome the OPF problem where in some studies, the OPF problem was solved by combining constraint handling (CH) techniques and self-adaptive (SP) penalty functions and integrating them into the differential evolution (ECHT-DE) algorithm. Particle swarm optimization (PSO) [23] algorithm has also been successfully applied to the OPF problem. The global best solution and inertia-weighted PSO (GWPSO) [24], improved particle swarm optimization (IPSO) [25], evolving ant-directed particle swarm optimization (EADPSO) [26], stochastic weight trade-off particle swarm optimization (SWT-PSO) [27] and parallel metaheuristics for graphics processing units (GPU-PSO) [28] are PSO based methods to solve the OPF problem. In Ref. [24], the inertia weighting factor was used to find the best solution quickly. In Ref. [25], the solution was reached by updating the weight factors with chaotic formulations. In Ref. [26], various models are introduced to improve the convergence speed. In Ref. [27], SWT-PSO is presented to improve the algorithm search capabilities by maintaining the balance between global exploration and local exploitation. In Ref. [28], a parallel optimal power flow solver, is proposed to run entirely on graphics processing units (GPUs) using a particle swarm optimization (PSO) algorithm. Furthermore, Naderi et al. proposed a multi-purpose OPF solution that incorporates objectives, such as fuel cost, active power losses, and emissions, within a novel fuzzy adaptive hybrid FAHSPSO-DE algorithm. This algorithm employs a self-adaptive particle swarm optimization (SPSO) and differential evolution algorithms in three distinct test systems. (IEEE 30, 57, and 118) [29].

In addition to the aforementioned studies, further developed algorithms for solving the OPF problem can be listed as follows: biogeography-based optimization (BBO) and its versions by the authors, quasi-opposite biogeography-based optimization (QOBBO) and adaptive real-coded biogeography-based optimization (ARCBBO) [30–32]. The gravity search algorithm (GSA) [33] by Duman et al. was subsequently employed by Bhownik et al. to enhance the existing population and accelerate the convergence of optimal solutions. This was achieved by incorporating adversarial learning, which enabled the identification and management of the Pareto frontier. The optimal frontier is then solved using the opposition-based gravity search algorithm (NSMOGSA) [34] and the non-dominated sorting multi-objective opposition-based gravitational search algorithm (NSMOOGSA) [35], which are both capable of solving the single and multi-objective OPF problem. Following the work of Sivasubramani and Swarup, who employed the harmony search algorithm (HS) [36] to address the multi-objective OPF challenge, the enhanced harmony search method (IHS) [37] was proposed, which leverages the Taguchi method to refine the range of design parameters. Additionally, the chaotic self-adaptive differential harmony search algorithm (CDHS) [38], which was designed by incorporating a chaotic self-adaptive differential mutation operator in lieu of the pitch adjustment operator to enhance the search capacity of the harmony search algorithm, was proposed. The artificial bee colony algorithm (ABC) was initially proposed by Karaboga in 2005 [39]. Subsequently, it was employed by Adaryani and A. Karami to address the challenging OPF problem [40]. Furthermore, it was proposed in Ref. [41] as an enhanced artificial bee colony algorithm (IABC). In the following years, new, more general, and reliable algorithms have been developed to solve the nonlinear OPF problem. The teaching-learning based optimization technique (TLBO) [42], first used by Abido et al. to solve the OPF problem, aims to reduce fuel cost, active power losses, and voltage deviation. Another version of TLBO, modified weighted teaching-learning based optimization (WTLBO) [43], has been proposed to solve the OPF problem. The results of the simulations demonstrate that WTLBO outperforms the original TLBO and other algorithms reported in the literature. The Lévy mutation teaching-learning based optimization (LTLBO) [44] algorithm, which employs the Lévy mutation strategy, has been shown to be capable of minimizing the optimal

settings of the control variables of the OPF problem on standard IEEE 30-bus and IEEE 57-bus test systems with different objective functions. With the advent of computers, heuristic optimization algorithms such as the modified bacterial foraging algorithm (MBFA) [45], the multi-objective modified imperialist competitive algorithm (MOMICA) [46], and the grey wolf optimizer (GWO) [47] have been employed to address single and multi-objective OPF. Significant advances in swarm intelligence techniques represent the primary driving force for the use of the Grey Wolf Optimizer (GWO) algorithm to solve the OPF problem. In the following years, a new crossover-search-based grey wolf optimizer (CS-GWO) [48] was proposed, in which the predation process in GWO was modified by first introducing a greedy mechanism and then a horizontal crossover operator was added to improve the first three. In the literature, various population-based solutions have been proposed, including the bird swarm algorithm (BSA) [49], moth swarm algorithm (MSA) [50], differential search algorithm (DSA) [51], backtracking search algorithm (BSA) [52], and metaheuristic approaches such as the search for symbiotic organisms (SOS) [53], the breeding krill swarm (SKH) algorithm [54], the opposition-based krill swarm algorithm (OKHA) [55], and the water evaporation algorithm (WEA) [56] have been proposed as potential solutions to address OPF.

In recent years, researchers have concentrated their efforts on the development of more efficient algorithms for tuning decision water evaporation algorithm: A new metaheuristic algorithm towards the solution of optimal power flow parameters and identifying the optimal solution. A number of techniques have been proposed, including the moth flame optimizer (MFO) [57], the improvement moth flame optimizer (IMFO) [58], the fast convergent Jaya algorithm [59], the adaptive multi-tool perturbation router Jaya (AMTG-JAYA) [60], new Sine-Cosine algorithm (MSCA) [61], and enhanced computational optimizer of social network search technique (ESNST) [62] have been used to solve large scale OPF problem.

The field of OPF research is expanding with the advent of advanced optimization methods in both machine learning [63] and artificial intelligence, leading to more advanced algorithms with global search abilities [64], such as evolutionary algorithms, swarm algorithms, and other heuristic algorithms [65,66]. For instance, in Ref. [65], a modified crow search optimization tool (MCSO) has been proposed to solve the coupled economic emission power flow (EEPF) problem. In Refs. [66,67], Salma Abd el-Sattar et al. and Zhu et al. proposed new optimization approaches, namely the Salp swarm algorithm (ISSA) and coyote optimization (COA) algorithm, respectively, to solve the optimal power flow problem. In Ref. [68], Su et al. adapted the cross-entropy method with chaotic operator (CGSCE), which has proven to be highly effective in addressing practical issues, to the OPF problem.

In [69], Manzoor Ahmad et al. used an effective methodology, called Orthogonal Experimental Design (OED), to solve the OPF problem by integrating it with the Bird Swarm Algorithm (IBSA). The OPF problem was successfully solved using the Successive History-based Adaptive Differential Evolutionary (SHADE) algorithm in Ref. [70] and the Improved Constrained Adaptive Differential Evolution (ICAD) algorithm in Ref. [71]. In Ref. [72], Mandeep Kaur et al. utilized the space transformational invasive weed optimization (ST-IWO) algorithm, a combination of invasive weed optimization (IWO) and space transformation search (STS) techniques, to address single and multi-objective optimal power flow problems. In Ref. [73], Shaheen et al. made two changes to the standard jellyfish search optimizer (JFS) algorithm in their proposed algorithm, called Semi- Quasi-Reflected Jellyfish Search Optimizer (QRJFS). They examined thirteen cases with economic, environmental, and technical objectives in four test systems and showed the superiority of their proposed algorithm. In Refs. [74,75], Okdağ et al. proposed new optimization approaches, namely the Harris Hawks optimization (HHO) algorithm and Improved Archimedes Optimization Algorithm (IAOA), respectively. Additionally, the OPF problem is addressed using hybrid algorithms proposed in Refs. [76,77], namely the Hybrid Approach with Combining Cuckoo Search and Grey Wolf (HCSGWO) and Optimal Power Flow Employing a Hybrid Sine Cosine-Grey Wolf Optimizer (HSC-GWO), respectively. In Ref. [78], the Arithmetic Optimization Algorithm (AOA) and Aquila Optimizer (AO) solvers, namely the AO-AOA, are applied to solve the Optimal Power Flow (OPF) problem, where the objective is to independently optimize the generation fuel cost, power loss, emission, voltage deviation, and L index. In Ref. [79], a Hybrid Differential Evolution and Harmony Search (Hybrid DE-HS) algorithm has been proposed for the OPF formulation, which includes active and reactive power constraints, prohibited zones, and valve point loading effects of generators.

Due to the nonlinear and non-convex nature of the optimal power flow (OPF) problem, finding the optimal solution using algorithms proposed in the literature takes time and effort. Researchers have developed various modifications and variants to existing algorithms to handle these drawbacks, including modified and combined methods. For example, in Ref. [80], Nguyen proposed a new social spider optimization algorithm (NISSO) for the OPF solution by making three changes in the traditional social spider optimization algorithm (SSO) to improve and accelerate the optimal solution quality. In Ref. [81], a Modified Artificial Hummingbird Algorithm (MAHA) has been proposed to effectively solve OPF and enhance the performance of the original Artificial Hummingbird Algorithm. In Ref. [82], a new variant of the Animal Migration Optimization (AMO) algorithm, known as Boundary Allocation Animal Migration Optimization (BA-AMO), was conceptualized to study the optimal power flow problem associated with IEEE bus systems.

OPF using solely thermal power generators has been the subject of in-depth research by scientists worldwide. Also, along with the improvement and necessity of including renewable energy systems, the study of OPF that takes into account the uncertainties of renewable sources becomes more important as wind power and other renewable plants can be integrated into the network. The uncertain nature of wind generation presents the largest obstacle to grid integration. Generally, private operators typically own the wind farms that an agreement is signed by the grid/independent system operator (ISO) to buy scheduled power from these private operators [83]. However, because the power output from these renewable sources is unpredictable, there's a chance that it will exceed the planned power, which could lead to an underestimate of the amount that is actually available.

The complexity of the problem increases even more when the uncertainty of power production from wind energy is included, in addition to the complexity brought about by the nonlinear constraints of the classical optimal power flow.

Among the OPF studies integrating wind energy in the past [45,84,85], are noteworthy. In Ref. [84], the Gbest-guided artificial bee colony (GABC) algorithm was proposed and found successful. The OPF problem was solved by a modified bacterial search algorithm (MBFA) with a model proposed for DFIG [45]. The authors proposed a paradigm for calculating the cost of wind-generated electricity

[85]. In Ref. [86], Devesh et al. proposed an enhanced artificial bee colony (ABC) algorithm that employs Gaussian and Cauchy probability distributions to address OPF issues pertaining to wind farm-based squirrel cage induction generators. In Ref. [87], Man-Im et al. presented an improved particle swarm optimization (IPSO) algorithm that incorporates chaotic mutation and stochastic weights to address OPF challenges associated with wind power uncertainty. In Ref. [88], Kaymaz et al. proposed a novel approach based on the integration of Levy flights and the coyote optimization algorithm (COA) for the minimization of the total cost of wind-thermal power generation.

In OPF studies conducted to date, researchers tried to minimize the objective functions such as fuel cost, carbon emission, power loss, and voltage stability by optimizing control variables such as load tap changer ratios, generator active power values, busbar voltages, and shunt capacitance values. The upper and lower constraints of these parameters are significant for the power system's operational safety and play an active role in determining the optimum configuration parameters. Therefore, in OPF studies, the best minimization value of the target function is highly dependent on the constraint limit values of the parameters, and the parameters must be in the same constraint conditions when compared with other studies. However, it has been found in the literature that the same objective functions are tried to be minimized with different constraint values.

Behaviors of butterflies have also inspired some researchers to develop various optimization techniques. Monarch Butterfly Optimization (MBO) is proposed for solving OPF on the IEEE 30 and 118-bus test systems by Vivek Yadav et al. [89]. However, to do best of our knowledge, there seems no other butterfly optimization applied to the problem of power flow optimization. While this study proposes to use a simple yet powerful algorithm, modified effective butterfly optimizer (MEBO) as a part of the (EBOwithCMAR) [90], it further modifies some of its stages to adapt it into the power flow optimization problem. The MEBO is swarm-based unconstraint optimization algorithm where only the solution variables are bound constraints. However, the power flow problem requires many constraints parameters, other than the solution variables, to be in the limits of the power system and minimizing the objective function must not violate these limits. The proposed MEBO minimizes the target function determined in IEEE 30 bus and 57 bus standard test systems while ensuring the constraint parameters. The study presents a comparison of the results with other studies presented in the literature under the same constraint conditions. In this study, the IEEE 30 bus test system is also optimized in terms of fuel cost by incorporating two wind generators into the system. This is achieved by considering not only the cost of wind generation but also the cost of wind power reserve and penalties.

Following is an overview of the paper's main contributions:

- In this study, the MEBO algorithm, an effective method inspired by butterfly behavior, is proposed to be adapted to solve the OPF problem for the first time in literature.
- The proposed MEBO adds penalties to objective functions in order to have the system operate in feasible state.
- The performance of the MEBO algorithm has been demonstrated by comparing with the state of the art methods under the same conditions.
- The study highlights and also demonstrates the importance of constraint parameters so that the optimal power flow and system configuration highly depend on the constraint limits.
- The performance of MEBO on renewable integrated system is also shown to optimize the system, successfully.

2. Optimal power flow

In the OPF problem considered in this study, the main objective is optimizing single functions while fulfilling the constraints such as load flow, generation bus voltage magnitudes, load bus voltage magnitudes, shunt VAR capacitances, reactive power generations, and transformer taps settings.

The problem can be defined as:

Optimize: $f(x,u)$.

With the subject of: $g(x,u) = 0$ *and* $h(x,u) \leq 0$.

In accordance with

$$x = [P_{Gslack} V_L Q_G S_l] \tag{1}$$

where x indicates the state variables, including real generation power of the slack bus P_{Gslack}, voltage of the load bus V_L, reactive generation power Q_G and transmission line loading S_l

$$u = [P_G \;\; V_G \;\; Q_C \;\; T] \tag{2}$$

u represents the variable vector for the elements, including the real power P_G, generator voltage V_G, the output of shunt VAR compensators Q_C and settings of the tap changing transformers T, f *and* g represent the objective function and the load flow equations, respectively, h indicates the parameter limits of the system.

2.1. Constraints of the power system

In the OPF problem, finding the best fitness value of objective functions is subject to satisfying Active (real) power flow and reactive power flow equations are named as equality constraints, and Security constraints on transmission lines, operating limits of equipment, and voltage magnitude limits on load buses are named as inequality constraints, and their details are given below.

2.1.1. Active and reactive load flow equations constraints

The typical equations related to load flow, $g(x, u)$, in the literature, is given by,

$$P_{G_i} - P_{D_i} - \sum_{j=1}^{n} |V_i||V_j||Y_{ij}|\cos(\theta_{ij} - \delta_i + \delta_j) = 0 \tag{3}$$

$$Q_{G_i} - Q_{D_i} - \sum_{j=1}^{n} |V_i||V_j||Y_{ij}|\sin(\theta_{ij} - \delta_i + \delta_j) = 0 \tag{4}$$

where P_{Gi} and Q_{Gi} are the real and reactive generation power outputs, P_{Di} and Q_{Di} are the active load and reactive load demand of bus i, the bus admittance matrix elements are represented by θ_{ij}, and finally, n is the total bus number.

2.1.2. Inequality constraints

In power systems, stable and secure physical settings of equipment and operational boundary limits are reflected by inequality constraints. The operating limits of generators, shunt capacitors, transformers tap settings, security constraints on transmission lines, and voltage magnitude limits of load buses are referred to as inequality constraints. These constraints of limits $h(x, u,)$ security of the power system and categorized as follows.

2.1.3. Generator constraints

Active, reactive power outputs and bus voltages of the generators are restricted by their lower and upper limits and the formulations of generator constraints are given as follows,

$$V_{Gi}^{min} \le V_{Gi} \le V_{Gi}^{max}\ i = 1, \ldots\ldots\ldots, N_g \tag{5.a}$$

$$P_{Gi}^{min} \le P_{Gi} \le P_{Gi}^{max}\ i = 1, \ldots\ldots\ldots, N_g \tag{5.b}$$

$$Q_{Gi}^{min} \le Q_{Gi} \le Q_{Gi}^{max}\ i = 1, \ldots\ldots\ldots, N_g \tag{5.c}$$

where N_g defines the number of generators, including the slack bus.

2.1.4. Transformer constraints

The maximum and minimum limits of tap settings regarding the transformer is given by,

$$T_i^{\min} \le T_i \le T_i^{\max}, i = 1\ldots\ldots\ldots, N_T \tag{6}$$

2.1.5. Shunt VAR compensator constraints

The maximum and minimum reactive power that can be injected or absorbed by compensators are defined by the user as,

$$Q_{C_i}^{\min} \le Q_{C_i} \le Q_{C_i}^{\max}\ \mathrm{i} = 1\ldots\ldots\ldots, \mathrm{N}_{Q_C} \tag{7}$$

2.1.6. Security constraints

The load bus voltage constraints and the maximum value of loadability capacity of the transmission line are,

$$V_{L_i}^{\min} \le V_{L_i} \le V_{L_{ii}}^{\max}\ \mathrm{i} = 1, \ldots\ldots\ldots, \mathrm{N}_{V_L} \tag{8}$$

$$S_{L_i} \le S_{L_{ii}}^{\max}\ \mathrm{i} = 1, \ldots\ldots\ldots, \mathrm{N}_{S_l} \tag{9}$$

2.2. Objective functions

It is intended to optimize the power system control parameters using the proposed EBO method for single-objective functions, including minimizing fuel cost, reducing fuel emissions, enhancing voltage stability, minimizing power loss, and minimizing voltage deviation. Certain objective functions employed in this study are listed below.

2.2.1. Quadratic cost function (f_C)

The fuel costs regarding each generator unit are modelled by quadratic functions as:

$$f_C = \sum_{i=1}^{Ng} a_i + b_i P_{Gi} + c_i P_{Gi}^2 \tag{10}$$

where N_g is the total generator number; P_{Gi} is the generation of real power at bus i; a_i, b_i, and c_i are the weighting factors of the generating unit i.

2.2.2. Fuel cost emission (f_E)

For the satisfaction of increasing energy demand, it is inevitable to generate electrical energy, despite harmful gas emissions and the worsening of air pollution. Therefore, the aim of fuel emission optimization is to minimize the amount of harmful gases released into the atmosphere by optimizing atmosphere by optimizing the control variables of the system.

$$f_E = \sum_{i=1}^{N_g} \alpha_i + \beta_i P_{Gi} + \gamma_i P_{Gi}^2 + \xi_i \exp(\lambda_i P_{Gi}) \Big) \text{ ton} / \text{h} \tag{11}$$

where f_E is the total emission cost (ton/h) and α_i, β_i, γ_i, ξ_i and λ_i are the emission coefficients of the ith unit.

2.2.3. Voltage stability enhancement (f_{VSI})

Voltage stability refers to the capacity to adjust the voltage level of the load buses to a specific value or range under nominal conditions. Typically, the voltage stability index, L-index, ranges from zero (no load scenario) to one (voltage collapse scenario) at any given bus. The index provides the most precise estimation of power system voltage problems, allowing the system to steer clear of voltage collapse. This proposed objective function is utilized to improve voltage stability and avoid voltage collapse) [23],

$$f_{VSI} = \min\big(\max(L_j)\big)\ \mathrm{j} = 1, \ldots.., N_L \tag{12}$$

Certain bus types in a power system can be classified as generator (PV and slack bus) or load (PQ) buses. It is essential to distinguish all buses due to the relationship between voltage stability and security issues with reactive power dispatch. The L-index formulation used in this work is also provided [91],

$$I_{system} = \begin{bmatrix} I_L \\ I_G \end{bmatrix} = \begin{bmatrix} Y_{LL} Y_{LG} \\ Y_{GL} Y_{GG} \end{bmatrix} \begin{bmatrix} V_L \\ V_G \end{bmatrix} \tag{13.a}$$

Where L and G indicate load and generator, respectively,

$$\begin{bmatrix} V_L \\ I_G \end{bmatrix} = \begin{bmatrix} Z_{LL} - Z_{LL} Y_{LG} \\ Z_{LL} Y_{GL} Y_{GG} - Y_{GL} Z_{LL} Y_{LG} \end{bmatrix} \begin{bmatrix} V_L \\ V_G \end{bmatrix} \tag{13.b}$$

Here, $Z_{LL} = Y_{LL}^{-1}$. For any load bus $j \in L$, through equation (14), the voltage of the bus is known as:

$$\dot{V}_j = \sum_{i \in L} Z_{ji} \dot{I}_i + \sum_{k \in G} A_{jk} \dot{V}_k \tag{14}$$

$$\left(\mathrm{A} = -Z_{LL} Y_{LG} \text{ and } \dot{V}_{oj} = -\sum_{k \in G} A_{jk} V_k \right)$$

The indicator of the voltage stability of the load bus j will be easily obtained.

$$L_j = \left| 1 + \frac{\dot{V}_{oj}}{\dot{V}_j} \right| \tag{15}$$

2.2.4. Transmission real power losses (f_{PL})

The control parameters are optimized to minimize the real power loss. The real power losses for each transmission line can be calculated as,

$$f_{PL} = \sum_{i=1}^{N_L} g_i \left[V_k^2 + V_m^2 - 2 V_k V_m \cos(\delta_k - \delta_m) \right] \tag{16}$$

where N_L is the number of transmission lines; g_i is the conductance of the ith line; V_k and V_m are the voltage magnitude at the end buses k and m of the ith line, respectively, and δ_k and δ_m are the voltage phase angle at the end buses k and m.

2.2.5. Voltage deviation (f_{VD})

In the literature, it is desirable to maintain the voltage deviation limits usually within ±5 % of the nominal value and fix at 1 p.u if possible [90].The voltage deviation for load buses is calculated as follows:

$$f_{VD} = \sum_{i=1}^{N_{PQ}} |V_i - 1| \tag{17}$$

where N_{PQ} is the load bus number.

3. EBO (effective butterfly optimizer)

EBO is a dual population-based bio-inspired optimization technique, which is inspired by the mate-locating behaviors of male butterflies [92]. It uses two populations, X_1 and X_2 of population size PS_1 and PS_2 respectively. EBO starts with random initail populations ($X_1 = \{\overline{x}1_1, \overline{x}1_2, \ldots \overline{x}1_{PS_1}\}, X_2 = \{\overline{x}2_1, \overline{x}2_2, \ldots \overline{x}2_{PS_2}\}$), where elements of vectors, $\overline{x}2_z$ and $\overline{x}2_z$ are initialized at eq. (1) within the search domain. Then, a new candidate population, $S = \{\overline{s}_1, \overline{s}_2, \ldots \overline{s}_{\mathrm{PS1}}\}$ is generated after "criss-cross" or "towards-best" modification, defined in Eq. (19), and finalized in Eq. (21) where the dimensions to update are selected using a tuned-crossover probability [93], defined in Eq. (23). Consequently, a pair-wise comparison between $\overline{x}1_z$ and its candidate $\overline{s}_z$ is made for all solutions based on the fitness values. Better solutions are preserved in X_1 whereas the remaining vectors are put in X_2. Below is a brief explanation of each step above.

1. **Initialization:** A D-dimensional vector is used to represent each individual in both the populations. Initially, each variable of the vectors is generated randomly within its boundaries as shown below.

$$\begin{aligned} \overline{x}1_{z,j} &= x_{LB,j} + \mathrm{rand}_j\,(0,1) * \left(x_{UB,j} - x_{LB,j}\right) \forall j = 1, 2, \ldots D \\ \overline{x}2_{z,j} &= x_{LB,j} + \mathrm{rand}_j\,(0,1) * \left(x_{UB,j} - x_{LB,j}\right) \forall j = 1, 2, \ldots D \end{aligned} \tag{18}$$

where $\mathrm{rand}_j\,(0,1)$ is a uniform random number within 0 and $1, x_{LB,j}$ and $x_{UB,j}$ are the lower and upper bound of j^{th} decision variable of problem respectively.

2. **Modification:** Modification is the solution update phase where butterflies are randomly either in perching or patrolling state depending on the probabilities $prob_{perch}$ and $prob_{pat}$. During perching, crisscross modification is used, whereas during patrolling, towards-best modification is used as follows. Thus, any initial candidate solution, $\overline{v}_z$, is acquired using either crisscross or towards-best modification randomly, as following,

$$\begin{aligned} \overline{v}_z &= \overline{x}1_{cc_z} + F * \left(\overline{x}1_{r1_z} - (X_1 \cup X_2)_{r2_z}\right) \\ \overline{v}_z &= \overline{x}1_{\mathrm{best}\ z} + F * \left(\overline{x}1_{cc_z} - (X_1 \cup X_2)_{r2_z}\right) \end{aligned} \tag{19}$$

where $\left(\overline{x}1_{cc_z}, \overline{x}1_{r1_z}, \text{and } (X_1 \cup X_2)_{r2_z}\right)$ are distinct individual vectors. $\overline{x}1_{\mathrm{best}\ z}$ is a best-neighbor of z^{th} vector. F is a positive real number that controls the rate at which the population evolves. $X_1 \cup X_2$ is the union of the both the populations. $\overline{x}1_{cc_z}$ is called criss-cross neighbor of z^{th} vector which is calculated using Eq. (20).

$$\{cc_1, cc_2, \ldots cc_{PS_1}\} = \mathrm{randperm}\,(1, PS_1) \tag{20}$$

where $\mathrm{randperm}\,(1, PS_1)$ is a random permutation vector of elements between 1 and PS_1.

3. **Crossover:** In EBO, a modified version of Binomial crossover is used where the tuned-crossover probability CR [91] is not similar for all dimensions. Crossover probability for particular j, cr_j is calculated by Eqs. (22) and (23) and used in Eq. (21) to get the final candidate solution $\overline{s}_{z,j}$.

$$\overline{s}_{z,j} = \begin{cases} \overline{v}_{z,j}, & \text{if } \left(\mathrm{rand}_j\,(0,1) \le cr_j \text{ or } j = j_{\mathrm{rand}}\right) \\ \overline{x}_{z,j}, & \text{otherwise.} \end{cases} \tag{21}$$

$$n_j = \mathrm{rem}\left(D + j - j_{\mathrm{rand}}, \frac{D}{2}\right) \tag{22}$$

$$cr_j = CR * e^{-\frac{T}{D}} * n_j \tag{23}$$

where j_{rand} is a randomly chosen integer index which guarantees that $\overline{s}_{z,j}$ acquires at least one component from $\overline{v}_{z,j}$, $\mathrm{rem}\,(a, b)$ operator gives the remainder of division of a and b, T is a real number within range of $[0, 0.5]$. If $T = 0$, then this crossover method is reduced to binomial crossover.

4. **Selection:** In EBO, one-to-one individual selection at iteration t is used, where the objective function values $f_{\overline{v}_z}$ is compared against $f_{\overline{x}_z}$, and the better one is taken as member of new primary population $(X1)$ in the next iteration $t + 1$. The worse one $\overline{x}_z$, is selected for the X2 and it replaces the randomly selected vector in X2 in the next iteration $t + 1$.

3.1. Modified EBO

Modified EBO (MEBO) is proposed as part of the hybrid algorithm, introduced in EBOwithCMAR [90].Different the EBO, MEBO

Algorithm replaces Eq. (19) and Eq. (21) with Eq.24 and 25 to increase the diversity of the population and also an *archive* is used to keep the success history of all solutions, denoted by *archive.X*. As another difference, MEBO uses Success History Based Adaption (SHBA) to fine tune the internal parameters of EBO, F,CR,*Freq*, and T. In the algorithm, SHBA is achieved through a historical memory, *memory* with *memSize* to keep track of success history of params, *F, CR, Freq, T*. The param values are initialized to 0.7,0.5,0.5, and 0.1 respectively using initialize_*memory*( ) function.

Population X is initialized same as EBO using *initialize_solutions (.)* function. At each iteration, random parameter values from the success history are acquired for each solutions, which is done in *generate_params* (.) function, defined at Eq. (29). These param values are used in solution update phase where the candidate population $V = \{v_1, v_2, \ldots v_{PS}\}$ is generated by modifying the current population X randomly either using *perching_update*( ) or *patrolling_update*( ), defined at Eq. (24) and Eq. (25) respectively. The solution update lines also uses crossover probabilities, *cr*, computed for each solution using *cross_over_probs (.)* function, according to Eq. (23). The probability of being in perching or patrolling state is determined based on the $prob_{perch}$ and $prob_{pat}$, defined at Eq.26 and 27. As another key feature of MEBO, Linear Population Size Reduction (LPSR) is used to reduce the population linearly. At the end of each iteration, *reduce_population*( ) function, defined at Eq. (28), is used to remove the worst K solutions from population X. Also, the memory is updated with good param values, using *update_memory*( ), defined at Eq.30–33. Similarly, archive is updated using *update_archieve*( ) function where *archive.X* keep good solutions of X, in pair-wise comparison, with their objective values in *archive.FX*. When archive is full, random elements of archive is replaced. The steps below cover the formulations of explanations above.

Algorithm. Modified EBO (PS_{min}, PS_{max}, D, lb, ub, memSize, *archSize,* FE_{max})

Global: $X, V, fitX, fitV, CR, F, T, Freq, archive, memory, prob_{perch} = prob_{perch} = 0.5$

$PS \leftarrow PS_{max}$
$X \leftarrow$ initialize_solutions(PS, D, lb, ub) //X is the population of solutions as matrix
$fitX \leftarrow f(X)$ //f is objective function, working vectoral
$memory \leftarrow$ initialize_$memory(memSize)$//memory is tuple of columns [F, CR, T, Freq]
$archive \leftarrow$ initialize_$archive(archSize, D)$//archive is tuple [X, FX] , initially empty
$Gbest \leftarrow X[1]$ // $Gbest$ keep track of global best
repeat
  $[CR, F, T, Freq] \leftarrow$ generate_params($memory$) // at Eq.(29)
  allX=[archive.X; X] // allX is the current pop with the success history of X
for $i = 1{:}PS$
    $cr \leftarrow$ cross_over_probs(D) // at Eq.(23)
    r $\leftarrow$ rand
    if r $< prob_{perch}$
      $V[i] \leftarrow$ perching_update ($X[i], cr$, allX) // at Eq.(24)
      $op[i] \leftarrow 1$
    else if r $< prob_{perch} + prob_{pat}$
      $V[i] \leftarrow$ patrolling_update ($X[i], cr$) // at Eq.(25)
      $op[i] \leftarrow 2$
    V$\leftarrow$ bound_control (V)
    $fitV \leftarrow f(V)$
    $cFE = cFE + PS$
    $I = fitV < fitX$// I isindices of success
    $[prob_{perch}, prob_{pat}] \leftarrow calculate\_probs(op)$ // at Eq.(26-27)
    $archive \leftarrow$ update_$archive(archive, I)$
    $memory \leftarrow$ update_$memory(memory, I)$ // at Eq.(30)
    $X[I] \leftarrow V[I]$
    $fitX[I] \leftarrow fitV[I]$
    $[fitX, X, PS] \leftarrow reduce\_population(fitX, X, cFE, FE_{max}, PS_{min}, PS)$// at Eq.(28)
    $Gbest \leftarrow bestOf(Gbest, X)$
until maximumiteration

1. **Improved Perching and Patrolling:** The solution update lines are modified in perching and patrolling search phases at Eq (24) and Eq (25) respectively.

$$v_{z,j} = \begin{cases} x_{z,j} + F_z\left(x_{r1_z,j} - x_{z,j} + x_{r2_z,j} - \text{allX}_{r3,j}\right), \\ \quad \text{if } \left(\text{rand}_j\ (0,1) \le cr_{z,j} \text{ or } j = j_{\text{rand}}\right) \\ x_{z,j}, \\ \quad \text{otherwise.} \end{cases} \tag{24}$$

$$v_{z,j} = \begin{cases} x_{z,j} + F_z\left(x_{\text{best}_z,j} - x_{z,j} + x_{r1_z,j} - x_{r2_z,j}\right), \\ \quad \text{if } \left(\text{rand}_j\ (0,1) \le cr_{z,j} \text{ or } j = j_{\text{rand}}\right) \\ x_{z,j}, \\ \quad \text{otherwise.} \end{cases} \tag{25}$$

where *cr* and *allX* are defined in the algorithm, and $r1_z$, $r2_z$ and $r3_z$ are distinct integers.

2. **Selection of the $best_z$ solution:** A new selection is used for the $best_z$ individual. When the size of the population *PS* is greater than 2*D*, then, the $best_z$ is the best individual among the randomly chosen *D* individuals. Otherwise, the $best_z$ is the best solution among the randomly chosen 10% individuals.

3. **Calculation of prob** $_{\text{perch}}$ **and prob pat:** The probabilities, $prob_{\text{perch}}$ and $prob_{\text{pat}}$, are initially set to 0.5 and updated using *calculate_probs*( ) function, according to the improvement rate in objective function values, as formulated in Eq.26 and 27, .

$$I_i^{t+1} = \frac{\sum_{z=1,i}^{PS_1} \max\left(0, f_z^{t+1} - f_z^t\right)}{\sum_{z=1,i}^{PS_1} f_z^t} \tag{26}$$

$$\forall \overline{x}1_z \text{ upadated by } \begin{cases} \text{perching}, & \text{if } i = 1 \\ \text{patrolling}, & \text{if } i = 2. \end{cases}$$

Then, $prob_{\text{perch}}$ and $prob_{\text{pat}}$ are calculated as [9]

$$\begin{aligned} \text{prob}_{\text{perch}} &= \max\left(0.1, \min\left(0.9, \frac{I_1}{I_1 + I_2}\right)\right) \\ \text{prob}_{pat} &= 1 - \text{prob}_{\text{perch}} \end{aligned} \tag{27}$$

4. **Linear Reduction of Populaton:** Population size PS is reduced linearly at the end of each iteration by eliminating the some number of worst solutions in X and fitX according to fitness values. Here fitX is the vector of objective function values of the solutions in X. The new pop size PS^{t+1} is computed using Eq. (28) [94].

$$\begin{aligned} PS^{t+1} &= \text{round}\left(\left(\frac{PS_{\min} - PS_{\max}}{FE_{\max}}\right) * cFE\right) + PS_{\max} \\ [X, fitX] &= \text{remove\_worst\_K\_solutions}(X, fitX, K) \end{aligned} \tag{28}$$

where $PS_{\min}, PS_{\max}$ are the minimum and maximum pop sizes respectively, $FE_{\max}$ and cFE are the maximum number of function evaluations and current total function evaluations respectively, and $K = PS - PS^{t+1}$, which is the number of worst solutions to remove from X and $fitX$,.

5. **Adaptation of** F, $Freq$, CR **and** T**:** In the algorithm, an ensemble of parameter adaption techniques are used to auto-tune the parameter F. For parameters $Freq$, CR and T, SHBA is used to sample new parameter setting accordingly with [94]. First of all we discuss the steps of the proposed SHBA technique which provide an efficient way to generate new parameter setting.

   New parameter setting, CR_z, F_z, Freq_z, and T_z, associates with individual x_z is calculated by equations at Eq. (29) respectively.

$$\begin{aligned} CR_z &= M2\left(M_{CR,r}, 0.1\right) \\ F_z &= \text{randci}\left(M_{F,r}, 0.1\right) \\ \text{freq}_z &= \text{randci}\left(M_{CR,r}, 0.1\right) \\ T_z &= M2\left(M_{T,r}, 0.05\right) \end{aligned} \tag{29}$$

where M_{param} is the memory vector for param ϵ $\{CR, F, \text{Freq}, T\}$ and r is random integer from $[1, memSize]$, randci is the cauchy distributions and M2 is the multi-variate random distribution around the mean M_{param}, r and symmetric covariances with deviations given.

In S_i, the values of parameter are recorded which is used by successful individual to update their function value [94]. After that the content of memory is updated by using Eq. (30).

$$M_{i,d} = \text{mean}_{WA}\left(S_i\right) \text{ if } S_i \neq null, \forall i \epsilon \{CR, F, \text{Freq}, T\} \tag{30}$$

where $1 < d < memSize$ is the index of the memory to be updated. It is initialized to 1, and then increased by 1 whenever an index of memory is updated and if it is greater than, it is reset to 1. The $\text{mean}_{WA}(S_i)$ is calculated by using Eq. (31) [94].

$$\text{mean}_{WA}\left(S_i\right) = \frac{\sum_{\gamma=1}^{|S_i|} w_\gamma S_{i,\gamma}^2}{\sum_{\gamma=1}^{|S_i|} w_\gamma S_{i,\gamma}} \forall i \epsilon \{CR, F, \text{Freq}, T\} \tag{31}$$

where,

Table 1
IEEE 30 and 57 Bus test System.

	IEEE 30 Bus Test System			IEEE 57 Bus Test System		
Items	Quantity	Description	Range	Quantity	Description	Range
Buses	30	[96]		57	[97]	
Branches	41	[96]		80	[97]	
Generators	6	Buses:1(Slack),2,5,8,11,13 Voltages V_G[pu]	[0.95 1.1]	7	Buses:1(Slack),2,3,6,8,9,12 Voltages V_G[pu]	[0.94 1.06]
Shunt capacitors	9	Buses:10,12,15,17, 20,21,23,24,29 Q_C[MVAR]	[0.0 5 0.0]	3	Buses:18,25,53 Q_C[MVAR]for Case 1, Q_C[MVAR]for Case 2,	[(0 20),(0 20),(0 20)] [(0 10),(0 5.9), (0 6.3)]
Transformers	4	Buses:11, 12, 15, 36 Tap ratio T [pu]	[0.95 1.1]	17	Buses:19,20,31,35,36,37,41,46,54,58,59,65,66,71, 73,76,80 Tap ratio T [pu]	[0.95 1.1]
Load buses	24	Voltages V_L[pu for Case 1 for Case 2,]	[0.95 1.05] [0.95 1.1]		Voltages V_L[pu]	[0.94 1.06]
Control variables	24	Active power of generators (slack not including), Voltages of all generators, shunt capacitors and transformers tap ratios		33	Active power of generators (slack not including), Voltages of all generators, shunt capacitors and transformers tap ratios	

Table 2
Simulation results of case studies 1 and 2 on IEEE-30 bus test system.

		Fuel cost minimization		*Fuel emission*		*L-Index*		*Active Power Loss*		*Volt. Dev*
Items	Range	Case1	Case2	Case1	Case2	Case1	Case2	Case1	Case2	Case
P_{G2}	[20 80]	48.7161	48.6908	67.5578	67.4340	79.8016	79.9958	80.0000	80.0000	78.7015
P_{G5}	[15 50]	21.3768	21.3021	50.0000	50.0000	49.9825	49.9995	50.0000	50.0000	49.9772
P_{G8}	[10 35]	21.2110	21.0207	34.9999	35.0000	34.9969	34.9990	35.0000	35.0000	34.9674
P_{G11}	[10 30]	11.9185	11.8540	30.0000	30.0000	21.7554	23.4969	30.0000	30.0000	29.9316
P_{G13}	[12 40]	12.0000	12.0000	40.0000	40.0000	35.1672	34.2592	40.0000	40.0000	33.8041
V_1	[0.95 1.1]	1.0834	1.1000	1.0622	1.1000	1.0743	1.1000	1.0613	1.1000	1.0018
V_2	[0.95 1.1]	1.0444	1.0677	1.0263	1.0758	1.0178	1.0817	1.0173	1.0676	0.9610
V_5	[0.95 1.1]	1.0332	1.0614	1.0372	1.0782	0.9532	1.0046	1.0379	1.0799	1.0489
V_8	[0.95 1.1]	1.0480	1.0790	1.0439	1.0854	0.9674	0.9999	1.0543	1.0968	1.0035
V_{11}	[0.95 1.1]	1.0635	1.1000	1.0559	1.1000	0.9988	1.0780	1.0536	1.1000	1.0074
V_{13}	[0.95 1.1]	1.0397	1.1000	1.0495	1.1000	1.0905	1.0999	1.0523	1.1000	1.0181
$Q_{c\text{-}10}$	[0 5.0]	2.9615	5.0000	1.4261	2.2067	4.9914	4.9966	1.0119	2.0419	5.0000
$Q_{c\text{-}12}$	[0 5.0]	4.4938	5.0000	4.8553	5.0000	4.9929	5.0000	2.8272	5.0000	4.1953
$Q_{c\text{-}15}$	[0 5.0]	4.4155	5.0000	4.5640	4.9943	4.9999	4.9828	4.6802	4.9992	4.9981
$Q_{c\text{-}17}$	[0 5.0]	5.0000	5.0000	4.9738	5.0000	4.9957	4.9977	4.9989	5.0000	0.0003
$Q_{c\text{-}20}$	[0 5.0]	4.1660	4.8682	4.2107	4.2024	4.9413	5.0000	4.1609	4.2358	5.0000
$Q_{c\text{-}21}$	[0 5.0]	5.0000	5.0000	4.9809	4.9999	4.9931	4.9959	5.0000	5.0000	4.9940
$Q_{c\text{-}23}$	[0 5.0]	3.1012	3.6415	3.1799	3.1846	4.9974	4.9992	3.2555	3.1809	5.0000
$Q_{c\text{-}24}$	[0 5.0]	5.0000	5.0000	4.9994	5.0000	4.9707	4.8164	4.9998	5.0000	5.0000
$Q_{c\text{-}29}$	[0 5.0]	2.0303	2.0820	1.9034	1.8137	0.4317	0.0035	1.8972	1.8251	2.5494
T_{11}	[0.9 1.1]	1.0204	1.0211	1.0360	1.0334	0.9148	0.9133	1.0450	1.0352	1.0201
T_{12}	[0.9 1.1]	0.9330	0.9000	0.9117	0.9000	0.9023	0.9000	0.9000	0.9000	0.9000
T_{15}	[0.9 1.1]	0.9640	0.9722	0.9898	0.9847	1.0414	0.9714	0.9902	0.9859	1.0030
T_{36}	[0.9 1.1]	0.9717	0.9580	0.9744	0.9692	0.908	0.9036	0.9748	0.9706	0.9666
P_{G1}	[50 200]	177.1762	177.1119	64.0533	63.9211	67.8787	65.6014	51.4778	51.2271	60.0024
Q_{G1}	[−20 150]	2.6620	−16.6563	−5.4004	−10.1437	94.6846	38.9796	−5.4888	−10.3654	−19.9997
Q_{G2}	[-20 60]	20.3278	21.4846	7.2574	7.1699	−17.3857	54.4092	7.2843	6.9584	−16.4987
Q_{G5}	[-15 62.5]	25.7260	26.4092	21.6693	21.4107	−14.91	−14.5169	21.7777	21.4010	54.8354
Q_{G8}	[-15 48.7]	26.6544	28.9608	26.2197	26.1853	−14.994	−14.9386	26.4951	26.2543	35.5660
Q_{G11}	[-10 40]	10.5003	8.6375	10.1212	9.0090	−9.9457	−9.8764	10.3792	9.0518	4.5284
Q_{G13}	[-15 44.7]	−7.5285	1.3612	0.6394	0.9256	33.4634	5.8352	2.7093	0.9256	7.3737
f_C ($/h)		**800.3873**	**798.8947**	944.305	943.4690	948.4158	946.7279	967.6092	967.0115	951.7262
f_E (ton/h)		0.3664	0.3663	**0.2048**	**0.2047**	0.2144	0.2133	0.2073	0.2072	0.2093
f_{VSI}		0.1687	0.1526	0.1406	0.1279	**0.1287**	**0.1177**	0.1408	0.1277	0.1486
f_{PL} (MW)		8.9986	8.5795	3.2111	2.9551	6.4557	5.2662	**3.0777**	**2.8271**	3.9843
f_{VD} (p.u)		0.9167	2.0006	0.9070	2.0735	0.7292	1.7229	0.9047	2.0806	**0.0842**

$$w_\gamma = \frac{\triangle f_\gamma}{\sum_{\gamma=1}^{|S_i|} \triangle f_\gamma}$$

and $\Delta f_\gamma = \left| f_{\gamma,\text{old}} - f_{\gamma,\text{new}} \right|$.

At each iteration $t \epsilon [0, t_{\max}/2]$, two tangential approaches are used to generate the new value of F, decreasing nonadaptive tangential approach (Eq. (32)) and increasing adaptive tangential approach (Eq. (33)). One of these two approach is chosen randomly with equal probability to adapt F for each individual.

$$F_z^t = \frac{1}{2}\left(\tan\left(\pi(t+1))t+1\right)\right)\pi\frac{t_{\max}-t}{t_{\max}}+1\right) \tag{32}$$

$$F_z^t = \frac{1}{2}\left(\tan\left(2\pi\,\text{Freq}_z * t\right)\frac{t}{t_{\max}}+1\right) \tag{33}$$

where $t_{\max}$ is maximum allowed iteration, Freq_z is adapted by using SHBA.

3.2. Adaptation of MEBO for power flow constraints

In this study, MEBO is implemented as constraint bounded algorithm for solving OPF problem not only including solution constraints but also the system constraints, such as slack variable (P_{Gslack}), bus voltages(V_L) and reactive power generations(Q_G). Let the variable x denotes any solution vector and $Y = [V_L, Q_G]$ is the vector of constraint parameters, corresponding to the bus voltages and reactive power generations respectively. Then, the objective function value, $f(x)$, used at line-3 and line-20 of the algorithm, is updated by the sequential operations through (Eq.(34)–(37)) to give penalty to any violating bound.

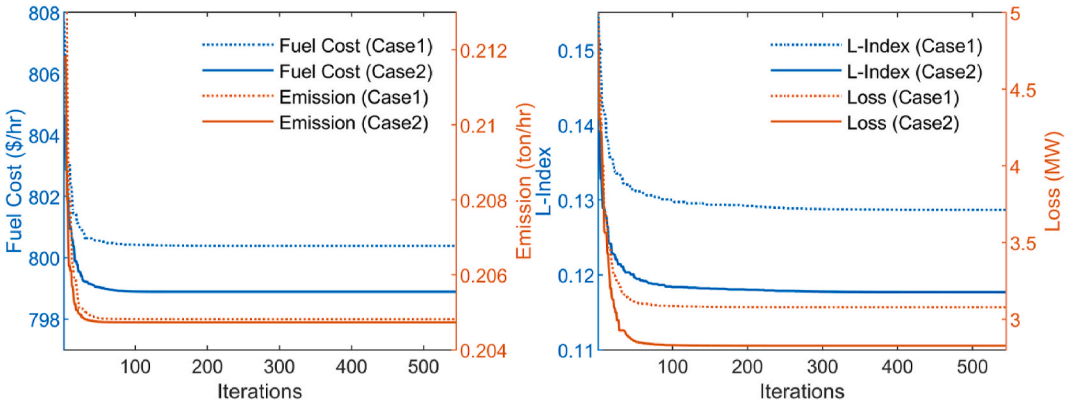

a) FuelCost and emission b) L-ındex and active power loss

Fig. 1. Convergence of the MEBO algorithm for objective functions.

$$[P_{Glsack}, Y] = PowerFlow(x) \tag{34}$$

$$P_{Glsack} = 1000 * P_{Glsack} * (P_{Glsack} > Ub_{Glsack} \| P_{Glsack} < Lb_{Glsack}) \tag{35}$$

$$Penalty(Y) = c * \sum_{i=1}^{n} [\text{abs}(Ub_i - \text{Y}_i) * (\text{Y}_i > Ub_i) + \text{abs}(Lb_i - \text{Y}_i) * (\text{Y}_i < Lb_i)] \tag{36}$$

$$f(x) = f(x) + Penalty(Y) \tag{37}$$

where $PowerFlow(x)$ function is [95], Ub_{Glsack} and Lb_{Glsack} are upper and lower bounds of the slack variable respectively, Ub_i and Lb_i are upper and lower bounds of the *i.* constraint parameters respectively and c is the penalty coefficient and empirically found for each objective function definition.

4. Description of the test system and case studies

In this paper, to assess the effectiveness of our proposed algorithm, we analyze two separate cases involving the widely used IEEE 30-bus and IEEE 57-bus test systems. We conduct a detailed comparison of the results obtained through our algorithm for both test systems using identical constraint values, as employed by existing algorithms within the literature.

The data, specifications, minimum and maximum operating constraints of both test systems are provided in Table 1. Further details can be found in Refs. [96,97]. Two case studies have been examined in the two IEEE grid systems to illustrate the subsequent points.

4.1. IEEE 30-bus test system

The system includes six generators, four transformers with off-nominal tap ratios at lines 6–9, 6–10, 4–12, and 28-27, and nine shunt compensators. The total system demand was 2.834 p.u for active power and 1.262 p.u for reactive power at 100 MVA base. The load demands are modelled as the fixed loads given in the literature. The details of coefficients for the fuel cost and emission cost are available in Ref. [22].

The upper and lower limits of the load bus voltages for the four objective functions were determined in the two case studies. That is, in the first case study (Case 1), all load buses were limited to 0.95 p.u - 1.05 p.u and in the second case study (Case 2), 0.95 p.u - 1.1 p.u. In the optimization of the voltage deviation function, only one case is studied for the voltages of the load busbars.

The optimized parameters that minimize the objective functions for each case with the proposed MEBO method are presented in Table 2. Details on the solution of five different objectives are given below.

Once Table 2 is examined, firstly the quadratic fuel cost minimization (f_C) is achieved with the optimum solution set converged by the MEBO optimization method. The total fuel cost is decreased to for case 1 and case 2800.3873 $/h and 798.8947 $/h, respectively. Proposed method has been shown remarkable performance. Secondly, the fuel emission minimization (f_E) of the IEEE 30 bus system is also investigated to obtain a more environmentally friendly solution set for the system parameters. As the third objective function, the minimization of the voltage stability index (f_{VSI}) of the system is investigated for both cases. Using the proposed EBO method, the L-index, i.e. the voltage stability index, is reduced to 0.1287 and 0.1177 for case 1 and case 2, respectively. Fourth, the proposed MEBO-based results of the optimal power flow problem for the objective function of minimizing the real power loss (f_{PL}) are documented for the system in Table 2. Using the proposed MEBO method reduces the active power loss to 3.0777 and 2.8271 MW for case 1 and case 2, respectively. As the final objective function (f_{VD}), voltage deviation optimization is considered for the OPF problem.

The MEBO method improves the total voltage deviation up to 0.0842. The system parameters of the solution set are presented in

Table 3
Wind farm and Weibull PDF parameters.

Parameter	Wind Farm 1	Wind Farm 2
Replaced Thermal Bus No	5	11
v_{in}(m/s)	3	3
v_r(m/s)	16	16
v_{out}(m/s)	25	25
Rated power[MW]	75	60
c – Weibull	9	10
k – Weibull	2	2

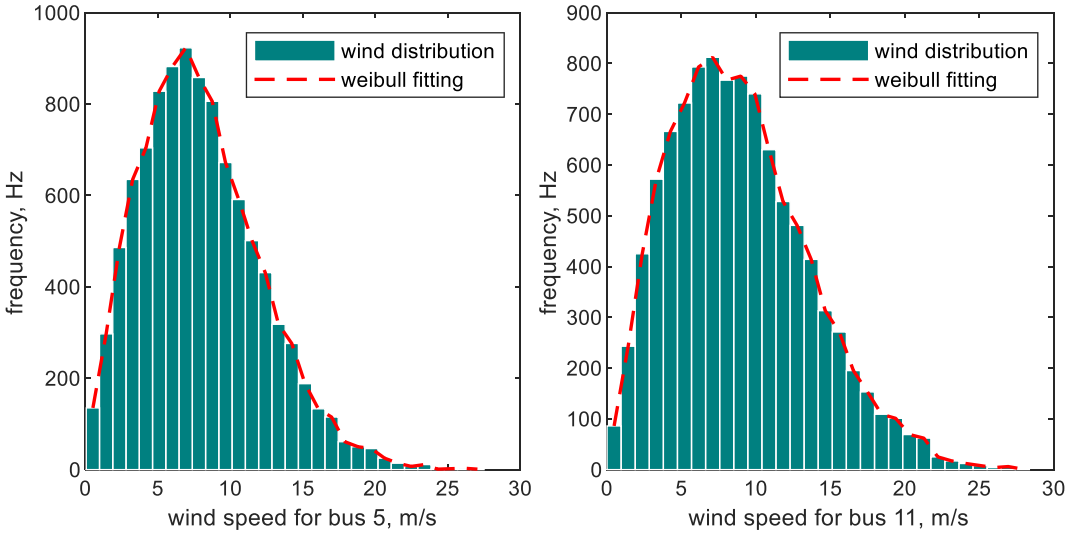

a) Wind farm integrated tobus 5 b) Wind farm integrated to bus 11

Fig. 2. Wind speed distribution for wind farms.

Table 2. Furthermore, Fig. 1 shows the convergence curves of the four objective functions in both cases and the proposed method converges faster in case 1, 2.

4.2. Modified IEEE 30- test system (renewable integrated system)

In this case, IEEE 30 bus test system is incorporated with 2 separate wind farms similar to other studies presented in literature [83]. For predicting the wind power depending on the wind speed, Weibull probability density function (PDF) is used. The Weibull PDF has 2 parameters namely c and k which are scale and shape factor, respectively. Also, in order to present the Weibull PDF of wind farm, the parameters of v_{in}, v_r and v_{out} which are cut-in, rated and cut-out speed should be determined. In this study, the wind generators are planned to be replaced in IEEE 30 bus power system instead of thermal generators in buses 5 and 11. The Weibull PDF parameters and wind farm parameters for corresponding buses are given in Table 3.

In order to employ the probability of wind speed v m/s by using Weibull PDF, equation (38) is given below where $f_v(v)$ is the wind speed probability.

$$f_v(v) = \left(\frac{k}{c}\right).\left(\frac{v}{c}\right)^{(k-1)}.e^{-(v/c)^k} \quad \{0 < v < \infty\} \tag{38}$$

Fig. 2a and 2b illustrate the optimal fit of the Weibull distribution, as determined through a Monte Carlo simulation with 10.000 iterations, for the frequency of wind output at buses 5 and 11, respectively using the k and c parameters required for the simulation of wind farms are presented in Table 3.

In wind power integration, if the wind farm produces less power than scheduled amount, a problem may occur due to over-estimating power from an uncertain source. For such situations, the system must operate out of schedule in order to provide the customers with uninterrupted supply. For wind farms, the reserve cost is the price of dedicating the reserve generating units to cover the overestimated amount. Another situation of operating wind farms is producing more power than scheduled amount. The excessive power would be wasted in such cases where the operator pays up penalty cost according to agreements [83]. In this study the direct wind power cost along with penalty and reserve cost is utilized. The direct cost function of wind farms along with the reserve and

Table 4
Simulation results of renewable case studies on IEEE-30 bus test system.

Items	Range	Case1	Case2
P_{G2}	[20 80]	41.3300	41.2749
$P_{G5}(Wind_1)$	[0 75]	42.1758	41.9948
P_{G8}	[10 35]	10.0001	10.0000
$P_{G11}(Wind_2)$	[0 60]	37.6250	37.5615
P_{G13}	[12 40]	12.0000	12.0000
V_1	[0.95 1.1]	1.0771	1.1000
V_2	[0.95 1.1]	1.0411	1.0686
V_5	[0.95 1.1]	1.0369	1.0677
V_8	[0.95 1.1]	1.0383	1.0813
V_{11}	[0.95 1.1]	1.0593	1.1000
V_{13}	[0.95 1.1]	1.0465	1.1000
$Q_{c\text{-}10}$	[0 5.0]	4.9275	5.0000
$Q_{c\text{-}12}$	[0 5.0]	2.9089	5.0000
$Q_{c\text{-}15}$	[0 5.0]	3.7641	5.0000
$Q_{c\text{-}17}$	[0 5.0]	4.9964	5.0000
$Q_{c\text{-}20}$	[0 5.0]	4.5870	4.8240
$Q_{c\text{-}21}$	[0 5.0]	5.0000	5.0000
$Q_{c\text{-}23}$	[0 5.0]	3.4254	3.4443
$Q_{c\text{-}24}$	[0 5.0]	4.9993	5.0000
$Q_{c\text{-}29}$	[0 5.0]	2.0131	1.9938
T_{11}	[0.9 1.1]	1.0029	1.0180
T_{12}	[0.9 1.1]	0.9533	0.9000
T_{15}	[0.9 1.1]	0.9718	0.9697
T_{36}	[0.9 1.1]	0.9706	0.9578
P_{G1}	[50 200]	146.6184	146.5675
Q_{G1}	[−20 150]	0.3672	−12.4990
Q_{G2}	[-20 60]	14.4686	15.1797
$Q_{G5}(Wind_1)$	[-30 35.0]	22.9773	23.2482
Q_{G8}	[-15 48.7]	26.6515	28.4212
$Q_{G11}(Wind_1)$	[-25 30]	7.0523	8.0098
Q_{G13}	[-15 44.7]	−2.5233	0.0828
$f_{Cthermal}$ ($/h)		549.0056	548.6708
f_{Cw1_direct} ($/h)		67.4811	67.1915
$f_{Cw1\_reserve}$ ($/h)		53.4090	53.0176
$f_{Cw1\_penalty}$ ($/h)		6.4194	6.4948
f_{Cw2_direct} ($/h)		60.1999	60.0992
$f_{Cw2\_reserve}$ ($/h)		45.0268	44.8937
$f_{Cw2\_penalty}$ ($/h)		5.4295	5.4559
f_{CTOTAL} ($/h)		**786.9717**	**785.8227**

penalty functions are given in equations (39)–(41), respectively.

$$C_{w,j}\left(P_{ws,j}\right) = g_j P_{ws,j} \tag{39}$$

$$\begin{aligned} C_{Rw,j}\left(P_{ws,j} - P_{wav,j}\right) &= K_{Rw,j}\left(P_{ws,j} - P_{wav,j}\right) \\ &= K_{Rw,j}\int_0^{P_{wsj}} \left(P_{ws,j} - p_{w,j}\right) f_w\left(p_{w,j}\right) dp_{w,j} \end{aligned} \tag{40}$$

$$\begin{aligned} C_{P_w,}\left(P_{wav,j} - P_{ws,j}\right) &= K_{Pw,j}\left(P_{wav,j} - P_{ws,j}\right) \\ &= K_{Pw,j}\int_{P_{ws,j}}^{P_{w,j}} \left(p_{w,j} - P_{ws,j}\right) f_w\left(p_{w,j}\right) dp_{wj} \end{aligned} \tag{41}$$

where, g_j, $K_{Rw,j}$ and $K_{Pw,j}$ are the direct cost coefficient, the reserve cost coefficient and the penalty cost coefficient for the j-th wind power plant, respectively. $P_{ws,j}$, $P_{wav,j}$ and $f_w\left(p_{w,j}\right)$ are the scheduled power, the actual available power and the wind power probability density function associated with j-th from the same plant, respectively. The total cost of wind power $\left(f_{cw}\right)$ generated from wind farms is described as follows;

$$f_{cw} = \sum_{j=1}^{N_{wG}} \left[C_{w,j}\left(P_{wsjj}\right) + C_{Rw,j}\left(P_{ws,j} - P_{wwv,j}\right) + C_{Pwj}\left(P_{wwv,j} - P_{ws,j}\right)\right] \tag{42}$$

By replacing the 2 thermal generators with wind farms, thermal and renewable cost optimization is applied by using OPF for two

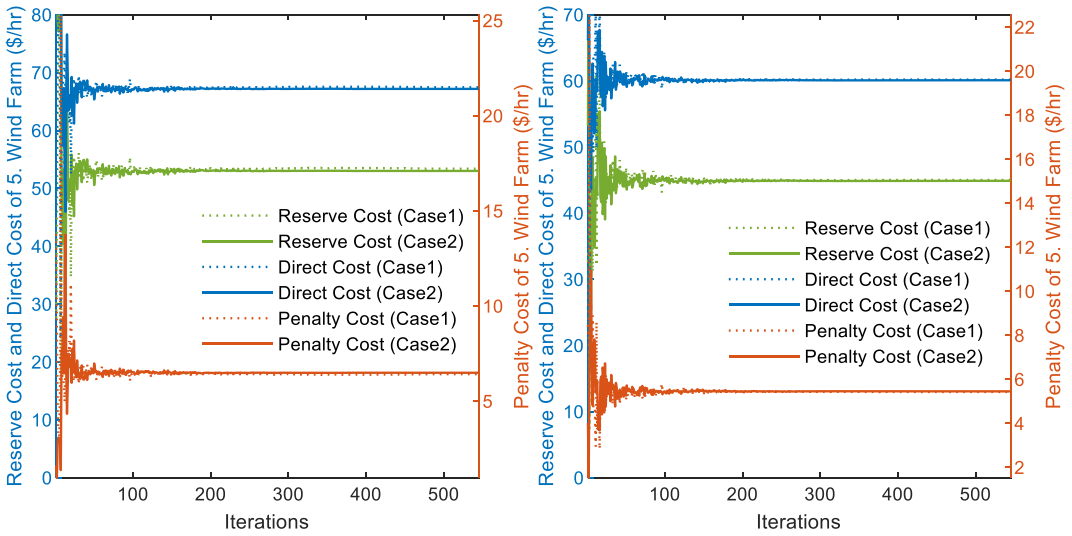

a) Cost values of wind farm 1 for both cases b) Cost values of wind farm 2 for both cases

Fig. 3. Convergence of the direct, reserve and penalty cost of wind farms.

different cases of load bus voltage values kept between 0.95 – 1.05 pu and 0.95–1.1 pu. Also, the active power constraints of the buses 5 and 11 are adjusted to 0–75 MW and 0–60 MW, respectively which are the minimum and maximum power outputs of wind farms. The results are presented in Table 4 where the total fuel cost for cases 1 and 2 are obtained by 786.9717 and 785.8227, respectively. Compared to the LCOA [88] presented in the literature at the same constraint values, the total cost is reduced from 792.2239 ($/h) to 786.9717 ($/h), confirming the superiority of MEBO in solution performance. Also, the convergence charts of direct, reserve and penalty costs of wind farms are given in Fig. 3, respectively.

4.3. IEEE 57-bus test system

The IEEE-57 bus test system has capacity of 1250.8 MW active power demand and 336.4 MVAr reactive power demand. It is utilized for simulation purposes and its detailed characteristics can be found in Table 1.

The minimum and maximum voltage magnitudes of all buses were considered to be 0.94 and 1.06 in p.u respectively. The system includes 7 generators, 17 transformers with off-nominal tap ratios and 3 shunt compensators. In the two case studies, the upper and lower limits of the shunt compensators for the five objective functions were determined. In the first case study (Case 1), all shunt compensators were limited at 0.0 MVAr - 20.0 MVAr. In the second case study (Case 2), shunt compensators were limited at bus no 18 to 0.0 MVAr −10.0 MVAr, at bus no 25 to 0.0 MVAr −5.9 MVAr, at bus no 53 to 0.0 MVAr −6.3 MVAr. The details of coefficients for the fuel cost and emission cost are available in Ref. [22].

The optimized parameters that minimize the objective functions for each case with the proposed MEBO method are presented in Table 5. After reviewing Table 5, we first achieved the minimum quadratic fuel cost (f_C) using the EBO optimization method within the constraints, resulting in a reduction in total fuel costs to 41676.65 $/h and 41685.97 $/h for case 1 and case, respectively. The proposed method exhibited remarkable performance. Secondarily, we analyzed the minimization of fuel emissions (f_E) in the IEEE 57 bus system to obtain a more environmentally friendly solution set for the system parameters. Also, fuel emission optimization for IEEE-57 bus is by using MEBO method. The proposed MEBO method converges to the total fuel emission of 0.9540 (p.u) and 0.9545 (p.u) for case 1 and case 2, respectively. The third objective function explores minimizing the voltage stability index (f_{VSI}) of the system in both case studies. Results indicate that utilizing the proposed MEBO method has reduced the L-index, otherwise known as the voltage stability index, to 0.1734 and 0.1764 for case 1 and case 2, respectively. Table 5 documents the proposed MEBO-based results of the optimal power flow problem for the objective function of minimizing the real power loss (f_{PL}) for the system. The MEBO method decreases active power loss to 9.9273 MW and 10.1039 MW for case 1 and case 2, respectively. For the OPF problem, voltage deviation optimization is considered as the final objective function, with the MEBO method improving total voltage deviation by up to 0.5962 and 0.6657 for case 1 and case 2, respectively. The solution set's system parameters are displayed in Table 5. Furthermore, Fig. 4 illustrates the convergence curves of the four objective functions in both cases, with the proposed approach converging faster in cases 1 and 2. It is evident that the proposed method provides a more efficient solution.

Table 5
Simulation results of case studies 1 and 2 on IEEE-57 bus test system.

		Fuel cost min.		*Fuel emission*		*L-Index*		*Active power loss*		*Voltage deviation*	
Items	Range	Case1	Case2	Case1	Case2	Case1	Case2	Case1	Case2	Case1	Case2
P_{G2}	[30 100]	90.2459	90.4231	99.9998	100.0000	85.2966	75.4946	5.7908	1.3185	50.5322	67.4310
P_{G3}	[40 140]	45.0210	45.0010	140.0000	140.0000	117.0970	113.0558	139.6942	139.6873	70.1650	75.9252
P_{G6}	[30 100]	71.2016	72.2115	99.9995	99.9968	52.3359	76.3819	99.6083	99.9949	8.1446	7.7678
P_{G8}	[100 550]	459.3576	459.0682	275.4885	274.6486	320.7498	287.5010	309.8781	307.0386	399.8846	366.5327
P_{G9}	[30 100]	96.8510	95.8148	100.0000	100.0000	93.5473	96.4994	99.9970	99.9999	79.8858	91.8238
P_{G12}	[100 410]	360.3430	360.7334	355.1449	355.6976	405.1165	398.8190	409.9189	409.9962	338.1392	263.2205
V_1	[0.94 1.06]	1.0575	1.0570	1.0598	1.0599	1.0533	1.0591	1.0595	1.0600	1.0183	1.0210
V_2	[0.94 1.06]	1.0555	1.0550	1.0600	1.0600	1.0383	1.0534	1.0539	1.0546	1.0411	0.9963
V_3	[0.94 1.06]	1.0489	1.0485	1.0591	1.0585	1.0591	1.0546	1.0572	1.0597	1.0129	1.0325
V_6	[0.94 1.06]	1.0573	1.0570	1.0541	1.0518	1.0467	1.0300	1.0581	1.0574	0.9912	0.9902
V_8	[0.94 1.06]	1.0600	1.0600	1.0568	1.0524	1.0580	1.0581	1.0598	1.0600	1.0135	1.0255
V_9	[0.94 1.06]	1.0370	1.0354	1.0164	1.0512	1.0464	1.0335	1.0599	1.0497	1.0336	1.0075
V_{13}	[0.94 1.06]	1.0404	1.0403	1.0405	1.0373	1.0597	1.0596	1.0459	1.0475	1.0343	1.0281
$Q_{c\text{-}18}$	[0 20][0 10]	10.5505	5.0744	15.0366	1.9831	19.8203	9.6719	8.1926	6.7177	4.4166	2.3184
$Q_{c\text{-}25}$	[0 20][0 5.9]	16.1351	5.8999	16.6887	5.8946	19.9767	5.8328	15.8043	5.8545	19.6658	5.5331
$Q_{c\text{-}53}$	[0 20][0 6.3]	14.9695	6.2980	13.1633	6.2706	19.5858	2.9232	14.3145	6.2958	19.8631	6.1258
$T_{4\text{-}18}$	[0.9 1.1]	0.9759	0.9675	0.9572	0.9997	1.0113	1.0908	1.0178	0.9730	1.0053	1.0254
$T_{4\text{-}18}$	[0.9 1.1]	0.9942	0.9858	1.0254	1.0388	1.0190	0.9549	0.9772	0.9976	0.9949	0.9811
$T_{21\text{-}20}$	[0.9 1.1]	1.0101	1.0105	1.0183	1.0531	0.9601	1.0034	1.0137	1.0153	0.9675	0.9659
$T_{24\text{-}25}$	[0.9 1.1]	1.0059	0.9597	1.0722	0.9306	1.0554	0.9660	1.0050	0.9533	1.0808	0.9536
$T_{24\text{-}25}$	[0.9 1.1]	1.0312	0.9444	0.9681	0.9657	1.0147	0.9871	1.0140	0.9431	1.0373	0.9879
$T_{24\text{-}26}$	[0.9 1.1]	1.0245	1.0262	1.0117	1.0094	1.0371	1.0704	1.0113	1.0132	1.0004	1.0328
$T_{7\text{-}29}$	[0.9 1.1]	0.9887	0.9798	0.9854	0.9749	0.9815	0.9588	0.9904	0.9809	0.9913	0.9599
$T_{34\text{-}32}$	[0.9 1.1]	0.9620	0.9399	0.9528	0.9390	1.0318	0.9985	0.9648	0.9353	0.9174	0.9182
$T_{11\text{-}41}$	[0.9 1.1]	0.9019	0.9003	0.9126	0.9001	0.9420	0.9433	0.9001	0.9087	0.9001	0.9001
$T_{15\text{-}45}$	[0.9 1.1]	0.9720	0.9694	0.9786	0.9764	0.9829	0.9806	0.9780	0.9777	0.9291	0.9297
$T_{14\text{-}46}$	[0.9 1.1]	0.9566	0.9533	0.9613	0.9527	0.9682	0.9634	0.9624	0.9600	0.9749	0.9679
$T_{10\text{-}51}$	[0.9 1.1]	0.9642	0.9632	0.9688	0.9624	0.9924	0.9898	0.9689	0.9705	1.0138	1.0049
$T_{13\text{-}49}$	[0.9 1.1]	0.9298	0.9253	0.9290	0.9149	0.9055	0.9036	0.9347	0.9276	0.9001	0.9008
$T_{11\text{-}43}$	[0.9 1.1]	0.9630	0.9603	0.9624	0.9578	0.9885	0.9830	0.9702	0.9659	0.9647	0.9575
$T_{40\text{-}56}$	[0.9 1.1]	0.9888	0.9959	0.9886	1.0033	0.9019	0.9047	0.9949	0.9816	0.9895	1.0076
$T_{39\text{-}57}$	[0.9 1.1]	0.9690	0.9666	0.9679	0.9715	0.9106	0.9012	0.9658	0.9723	0.9001	0.9021
$T_{9\text{-}55}$	[0.9 1.1]	0.9857	0.9795	0.9769	0.9687	1.0626	1.0771	0.9771	0.9766	0.9848	0.9755
P_{G1}	[0575.88]	142.8454	142.8258	193.1531	193.6725	189.5276	216.4729	195.8399	202.8685	323.3897	403.8415
Q_{G1}	[−20 150]	46.6631	47.0636	31.9888	37.7863	18.8190	28.4946	37.9192	34.1407	4.6928	0.0833
Q_{G2}	[-17 50]	49.9958	49.9996	48.3811	48.6472	19.2072	30.4647	49.8056	49.8888	33.8288	44.9611
Q_{G3}	[-10 60]	33.2988	39.5221	31.4023	43.9975	38.0925	33.7593	28.2526	37.9613	55.6254	53.5706
Q_{G6}	[−8 25]	9.8928	15.0456	−3.0815	4.9236	11.7745	10.4706	1.5024	2.1293	0.7093	−2.9956
Q_{G8}	[−40 200]	28.9095	38.1067	49.4038	53.0950	25.8280	59.3075	40.6832	48.6223	14.7762	63.4852
Q_{G9}	[-3 9]	9.0000	8.97978	8.9939	8.9893	8.3856	2.0585	8.9668	8.9973	8.9894	8.9612
Q_{G12}	[−150 155]	57.2379	61.6460	55.6374	57.0552	83.8953	86.5942	49.2629	54.3920	142.9000	147.6208
f_C ($/h)		**41676.65**	**41685.97**	45125.21	45147.75	43879.70	44258.95	44930.37	45032.75	44850.03	48315.60
f_E (ton/h)		1.9101	1.9076	**0.9540**	**0.9545**	1.3523	1.2971	1.3889	1.3976	1.7737	1.7454
f_{VSI}		0.2125	0.2265	0.1867	0.2239	**0.1734**	**0.1764**	0.1806	0.2202	0.1953	0.2217
f_{PL} (MW)		15.0655	15.2778	12.9858	13.2155	12.8707	13.4245	**9.9273**	**10.1039**	19.3409	25.7425
f_{VD} (p.u)		1.6243	1.5414	1.6354	1.5494	1.8038	1.7225	1.6712	1.6281	**0.5962**	**0.6657**

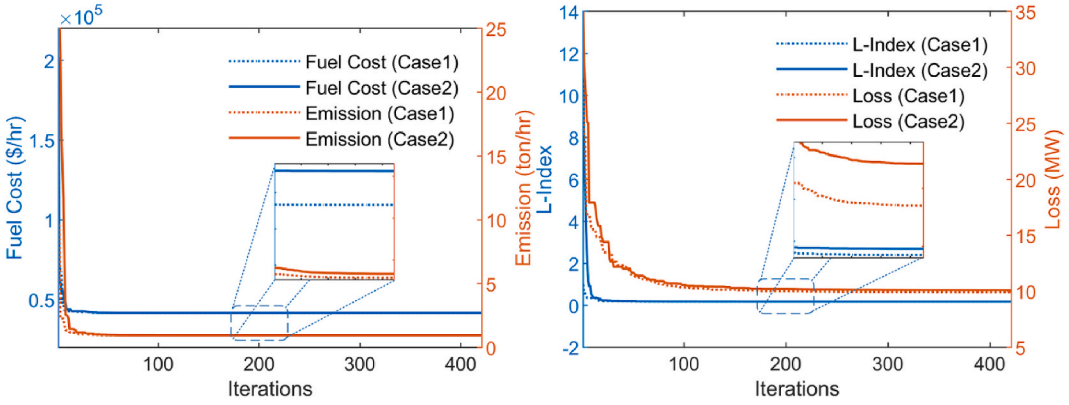

a) Fuelcost and emission b) L-index and active power loss

Fig. 4. Convergence of the MEBO algorithm for objective functions.

5. Validation of the proposed algorithm for OPF problem

5.1. Results compared with other reported literature

In this subsection, we compare the results acquired by MEBO with other state-of-the-art techniques reported in the literature. In Tables 6 and 7, the previous studies and the proposed method are compared for the same constraint values for systems with 30 and 57 buses, respectively, and it is clearly seen that the proposed optimization method achieves the best values compared to some other methods presented in the literature and given in these tables. In Tables 6 and it can be seen that for (f_C), the proposed method is superior to most of the methods such as ACDE [21], MSA [55], CGSCE [68], IєJADE [71], ARCBBO [32] and COA [67] for case 1; WEA [56] NISSO [80], NSGA-III [98], MOBSA [99], BSA [52], ICBO [100] and AQDMBBO [101] for case 2. From Tables 7 and it is seen that the proposed method for 57 bus system is superior to most of the methods such as GSA [33], LTLBO [44] SKH [54], NSGA-III [98], TSA [102], BA-AMO [82], MDE [103] for case 1 and ICBO [100] for case 2.

In Tables 6 and 7, there are some solutions obtained in literature namely infeasible solution. These solution sets labeled as ("*") due to one or more load and generators buses violating the constraints. In Table 6, such as AO-AOA [78], GSA [33], EGA-DQLF [15], MSCA [61], ST-IWO [72]; in Table 7, HCSGWO [76] infeasible solution labeled as "*".

In these tables, it is observed for 30 and 57 bus systems that the best L-index obtained by MEBO method is better than the other methods such as ACDE [21], NISSO [80], CGSCE [68], ECHT-DE [22], SKH [54], NSGA-III [98] and ESDE-MC [110]. Moreover, some methods such as AO-AOA [78] and BBO [30] for the 30-bus system are infeasible solutions.

Minimum power loss obtained by MEBO which is also less compared to other methods namely IABC [40], IBSA [69], IєJADE [71], TLBO [109], SKH [54] and DSA [51] for 30-bus system as seen in Table 6. Besides, AO-AOA [78] and ST-IWO [72] are labeled as infeasible solution due to violating the constraints of one or more load buses for the 30-bus system. For the 57-bus system, Table 7 shows that the proposed method obtains outperformance of some computations presented in the literature, such as ST-IWO [72], SKH [54], NSGA-III [98], TSA [102] BA-AMO [82] and ESDE-MC [110]. On the other hand, some methods given in literature like CGSCE [68], ST-IWO [72], HCSGWO [76] and ESDE-MC [110] converge to infeasible solution due to constraint violation in the 57-bus system.

In Table 6, when the voltage deviation for 30-bus system is compared with other methods in the literature, it can be seen that the proposed method outperforms most of the methods such as IABC [40], NISSO [80], HHO [74], LTLBO [44], NSGA-III [98], AQDMBBO [101], ARCBBO [32] and MPA [107]. It also exhibits better performance than CGSCE [68], ST-IWO [72], SKH [54], NSGA-III [98] and TSA [102] for the 57-bus system in Table 7.

5.2. Security constraint validation for MEBO

As previously mentioned in Section 2.3, operational safety is guaranteed by adhering to the permitted power and voltage limits for the generators. Additionally, the voltage values at the load buses must remain within the minimum and maximum limits. The generator reactive power limits are enforced when the voltage on the load buses approaches the upper limits. It is imperative to prevent limit violations in the OPF problem. This subsection presents a detailed representation of the safety limit values determined for the generator and load buses in the optimal solution set obtained by MEBO for each objective function.

For the safety of power systems, the voltage amplitudes of all buses must never exceed the permissible limits. To show that these constraints are agreed, the graphs in Fig. 5 are plotted in detail. In Fig. 5, it is clearly seen that the load bus voltage values for both cases of fuel cost, fuel emission, L-index and active power loss objective functions are below the blue colored dashed line (1.05 p.u) and dotted line (1.1 p.u) line limits, respectively. A careful examination of Fig. 5a, b, c, and d reveal that the bus voltages frequently approach their limits due to constraints in the load bus voltages, particularly in case 1. The scarcity of green areas indicates this situation. The voltage magnitudes of the proposed approach, which does not violate its constraints, appear to be within acceptable

Table 6
Results of the comparing to earlier studies in 30-bus system.

Case no	Methods	f_C	f_E	f_{VSI}	f_{PL}	f_{VD}
Case1	ARCBBO [32]	800.5159	0.2048	0.1369	3.1009	0.092
	SKH [54]	800.5141	0.2048	0.1366	3.0987	
	CGSCE [68]	800.5106	0.204823	0.13667	3.1006	
	MSA [55]	800.5099	0.20482		3.1005	
	COA [67]	800.5054		0.1244	3.0952	0.0826
	SSA [66]	800.4752				
	EO [104]	800.4235				
	IABC [40]	800.4215	0.1943[a]		3.0917	0.0918
	ECHT-DE [22]	800.4131	0.20482	0.13632		
	ACDE [21]	800.41132	0.204817	0.136447	3.084041	0.085636
	I€JADE [71]	800.4113	0.2048	0.1364	3.0840	0.0856
	C2oDE [105]	800.4113	0.20481	0.1367	3.08392	
	IBSA [69]	800.3975	0.20482		3.0828	
	DSA [51]	800.3887	0.2058255		3.09450	
	IMFO [58]	800.3848	0.2048		3.0905	
	AMTPG-JAYA [60]	800.1946[c]		0.1240	3.0802	
	AO-AOA [78]	800.0239[a1]	0.20482	0.12181	3.01791[a1]	0.101248
	AGOA [106] [a]	800.0212[b]	0.20484			
	CS-GWO [48]	799.9978			3.0861	
	ST-IWO [72]	799.73[a4]	0.2047		2.981	0.1019
	EGA-DQLF [15]	799.56[b]		0.10402	3.2008	
	MCSO [65] [a]	799.333[b]	0.204891			
	MSCA [61]	799.31[a3]			2.9334	0.1030
	BBO [30] [a]	799.1116[b]		0.09803		0.0951
	MPA [107]	799.0725[a2]		0.1131	2.8513	0.0992
	GSA [33] [a]	798.6751[b]		0.116247		0.09329
	MEBO	**800.3873**	**0.20481**	**0.1287**	**3.0777**	**0.0842**
Case 2	BHBO [108]	799.9217		0.11671	3.5035	
	HSC-GWO [77]	799.8755				
	LTLBO [44]	799.4369	0.2047			0.0974
	BA-AMO [82]	799.2458			2.8400	
	NSGA-III [98]	799.21	0.20482	0.1243	2.907	0.0953
	QRJFS [73]	799.1065	0.204688[d]		2.856711	
	ESNST [62]	799.0824	0.204681[d]		2.85076	
	BSA [52]	799.076				
	TLBO [109]	799.0715		0.11311		0.0945
	IAOA [75]	799.068	0.2045[d]		2.85	
	MOBSA [99]	799.046			2.8841	
	ICBO [100]	799.0353				
	ESDE-MC [110]	799.0313	0.2047	0.1241	2.8482	
	AQDMBBO [101]	799.0309	0.2047	0.0907	2.8423	0.1247
	WEA [56]	798.996			2.8604	0.0875
	NISSO [80]	798.9936	0.20479	0.12547	2.8678	0.09071
	IMRFO [111]	798.9888	0.204754	0.0927	2.846	
	HHO [74]	798.9105	0.21776		3.1069	0.1099
	CSD-HHO [74]	798.6955[b]	0.2194			
	Initial	901.99	0.239	0.2144	5.842	1.1606
	MEBO	**798.8947**	**0.20473**	**0.1177**	**2.8271**	**0.0842**

a2, a3 and a4.The load bus voltages constraint have been violated due to reported voltage deviations of 1.8516, 1.4246, and 1.65739, respectively.

[a] Infeasible solution (**[a1]** The constraint on load bus voltage is violated because the voltage deviation was reported as 2.04713. On the other hand, given that the total active power generation is stated as 286.4988 MW, the active power loss amounts to 3.0988 MW.

[b] Load bus voltages and generator reactive power output values cannot be verified as they are not reported).

[c] The active power limits of the generator were used in different ways.

[d] The active power values of generators don't verify the result.

limits. In contrast, there is a direct correlation between reactive power and voltage. Although the buses 10 and 12 have reactive power support, they reach the limit values, thereby confirming the optimum results found by the MEBO algorithm for these buses. Despite the high reactive power consumption in the bus number 21, the MEBO algorithm managed to keep the capacity powers injected into this bus below the determined voltage value by bringing them to maximum limit values.

Fig. 5 and 6 show the two important values such as load bus voltage and generator reactive power for IEEE 30 bus system. It is clear from Fig. 5 that the load bus voltages for both cases are within the limits set for objective functions. A careful examination of Fig. 5 a, b, c, d, it becomes evident that the bus voltages frequently approach their limits, particularly in case 1 due to constraints on the load bus voltages. The scarcity of green areas explains this situation. On the other hand, Table 2 shows that the voltage deviation values for objective functions (f_C), (f_E), (f_{VSI}), and (f_{PL}) are found to be 0.9167, 0.9870, 0.7292, 0.9047 for case 1 and 2.0006, 2.0735, 1.7229, 2.09870, 2.0806 for case 2, respectively. The results obtained for both cases confirm that all load buses remain within the permissible

Table 7
Results of the comparing to earlier studies in 57-bus system.

Case no	Methods	f_C	f_E	f_{VSI}	f_{PL}	f_{VD}
Case 1	TPCMaO [112]	41709.0	1.1733	0.2551	10.9192	0.6182
	GSA [33]	41695.8717				
	DSA [51]	41686.82				
	ARCBBO [32]	41686.00				
	TSA [102]	41685.07			12.4730	0.717
	MDE [103]	41682.00			10.2642	
	BA-AMO [82]	41679.83			10.026	0.659
	LTLBO [44]	41679.5451				
	SKH [54]	41676.9152		0.2721	10.6877	1.080
	NSGA-III [98]	41676.69		0.2551	10.010	0.6182
	ISSA [66]	41675.0203[a2]				
	MSA [55]	41673.7231[b3]				
	ESDE-MC [110]	41671.1431[b1]	1.0788	0.2718	10.788	
	ST-IWO [72]	41670.772[a3]	0.994		10.680	0.6882
	COA [67]	41668.35[b4]				
	CGSCE [68]	41667.2777[b5]				0.5880[b5]
	IMFO [58]	41667.1497[b2]				
	HCSGWO [76] [a]	41665.53[a1]	0.955	0.2331	8.880[a1]	
	C2oDE [105]	41662[b6]				0.58546
	AGOA [106]				11.812	0.7721
	MEBO	**41676.653**	**0.9540**	**0.1734**	**9.9273**	**0.5962**
Case 2	MATPOWER [113]	41737.79				
	ICBO [100]	41697.3324				
	MEBO	**41685.979**	**0.9545**	**0.1764**	**10.1039**	**0.6657**

[b2, b3, b4, b5] The load bus voltages cannot be verified as they are not reported, whereas the generator voltage falls within the range of 0.95–1.1.

[a] Infeasible solution ([a1] Load bus voltages, generator reactive power and slack generator active power output values cannot be verified as they are not reported. Shunt compensator values are between 0 and 30.0 MVAr. The load bus voltages cannot be verified as the generator reactive power output values are not reported. Since the voltage values V_1, V_2, V_8, V_9 in "[a2]"and V_6, V_8, V_9 in "[a3]" are higher than 1.06 p.u., the load bus voltage constraint is violated).

[b1] Generator voltage ranges between [0.95 1.1].

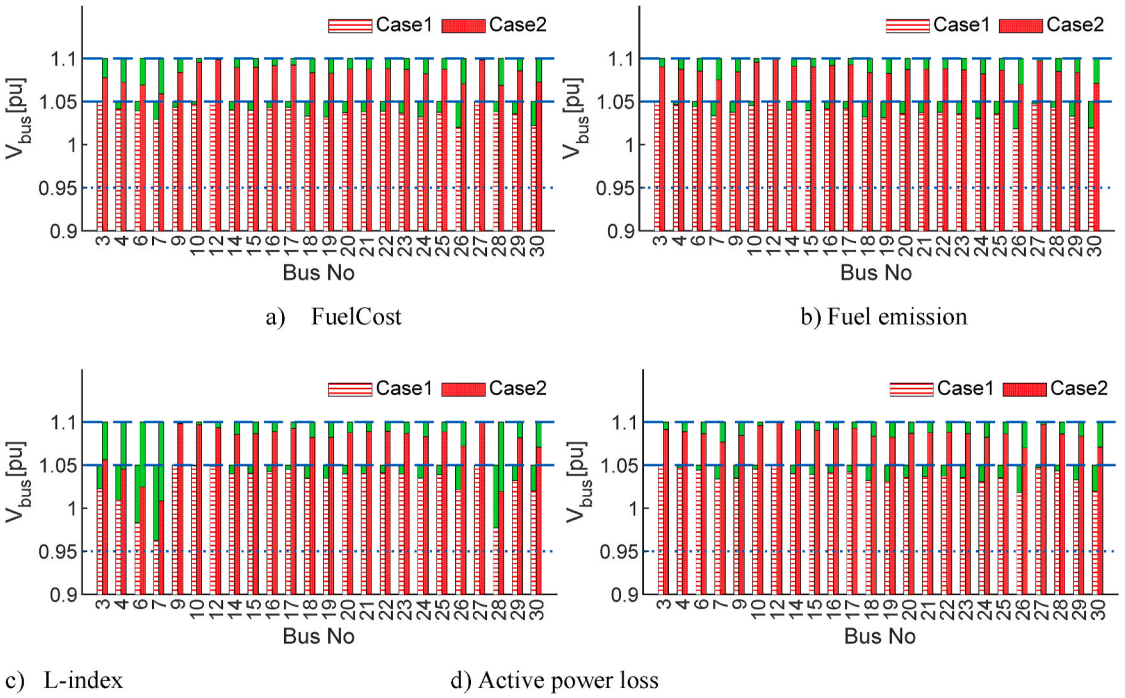

Fig. 5. Load bus voltages for IEEE 30 Bus system.

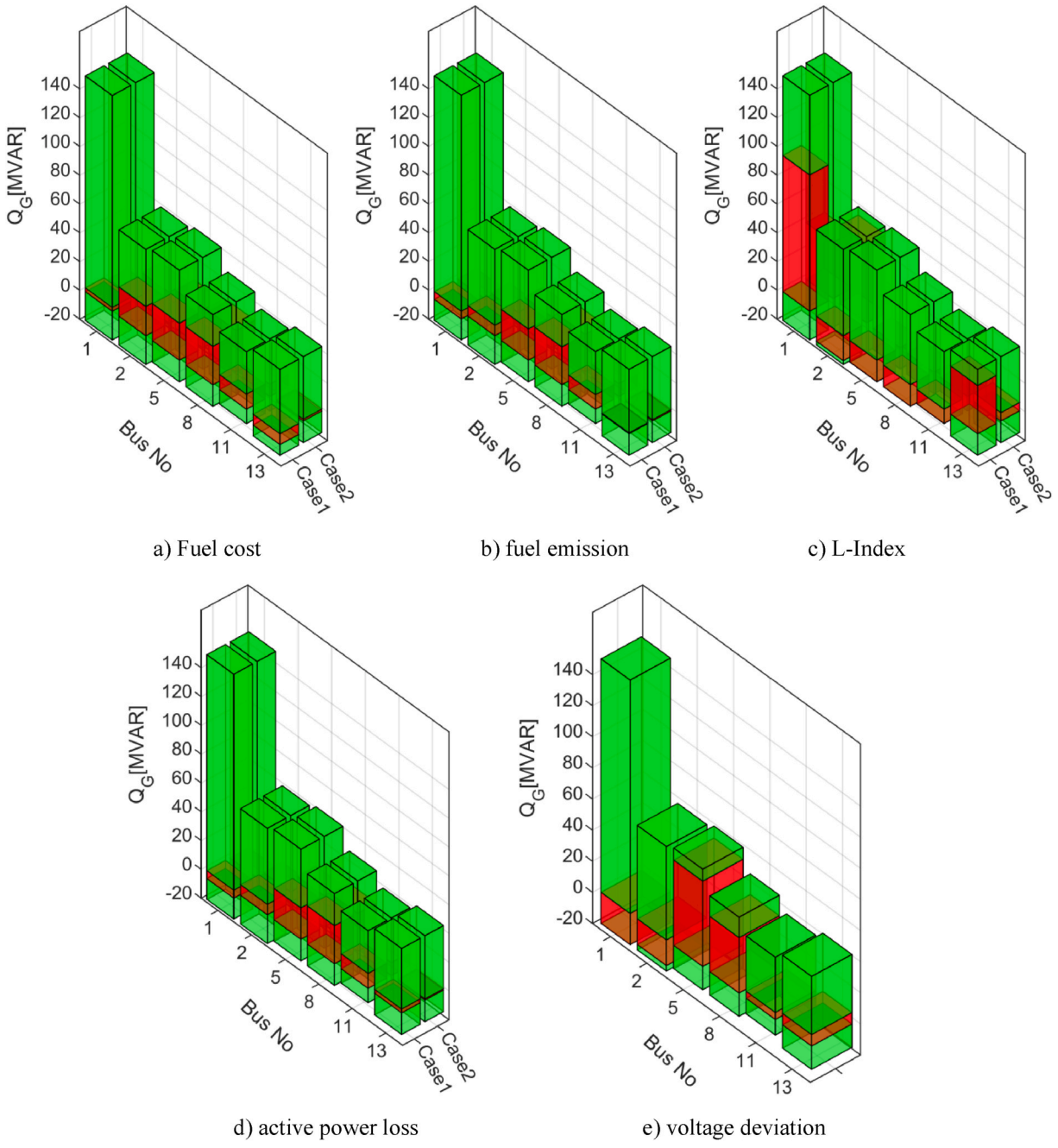

Fig. 6. Generator reactive power outputs for IEEE 30 Bus system.

limits. Regarding the objective function f_{VD} , analyzing only one case is enough. The overall voltage deviation of the buses is 0.0842.

Fig. 6 provides a lucid display of reactive power outputs for generators under five objective functions. The lengths of the green colored bars are in the range of the lower and upper limit values determined for the generator. The reactive power outputs of each generator are illustrated in red. A small green colored area depicts operation close to the lower or upper limits. It is clear from Fig. 6a, b, c that the generator reactive power outputs are far from the limit values. It is observed that generators 2, 5, 8 and 11 in Fig. 6 d and generators 1 and 2 in Fig. 6 e are close to the lower limit values and are under a stressful operating condition. Figs. 5 and 6 demonstrate that the MVAR outputs of the generators and the voltages of the load buses are within acceptable limits. The proposed method generates an exceptional set of solutions for five objective functions while observing the constraints in OPF problem solving.

It is clearly seen from Figs. 7 and 8 that the load bus voltages and generator reactive power limits are not violated for both cases in the 57-bus system. The load bus limit voltage values determined for the 57 bus system are between 0.94 and 1.06 p.u. It can be

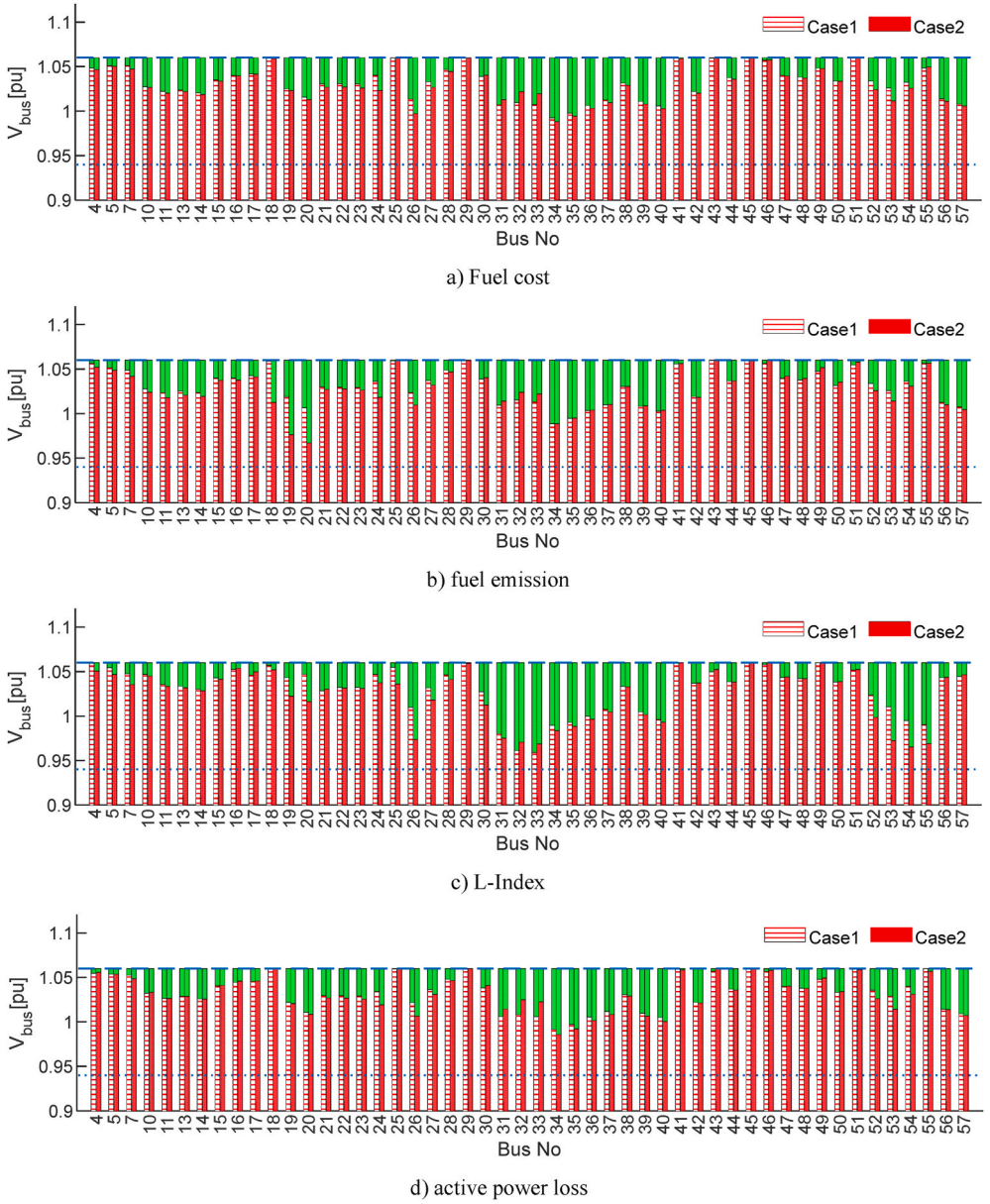

Fig. 7. Load bus voltages for IEEE 57 Bus system.

observed that there is a greater proportion of green area in this system compared to the 30 bus system. The proposed algorithm ensured that the shunt capacitors in busbars 18–25 and 53 remained within the specified limits. Meanwhile, Table 6 shows that the voltage deviation values for objective functions (f_C), (f_E), (f_{VSI}), and (f_{PL}) are found to be 1.6243, 1.6354, 1.8038, 1.6712 for case 1 and 1.5414,1.5494,1.7225,1.6281 for case 2, respectively. The results obtained for both cases confirm that all load buses remain within the permissible limits.

In the 57-bus system, as in the 30-bus system, the MVAR outputs of the generators and the voltages of the load buses are within acceptable limits, as demonstrated in Figs. 7 and 8. The proposed method yields an outstanding solution set for five objective functions while fulfilling the constraints in the OPF problem solution.

Fig. 8 reveals that generator 9 operates at the lower limit for all objective functions. Additionally, generators 2 and 12 operate close to the upper limits, as shown in Fig. 8a, b, 8d, and 8e.

6. Conclusions

This article presents a novel nature-inspired optimization approach, MEBO, which has been successfully applied to the OPF

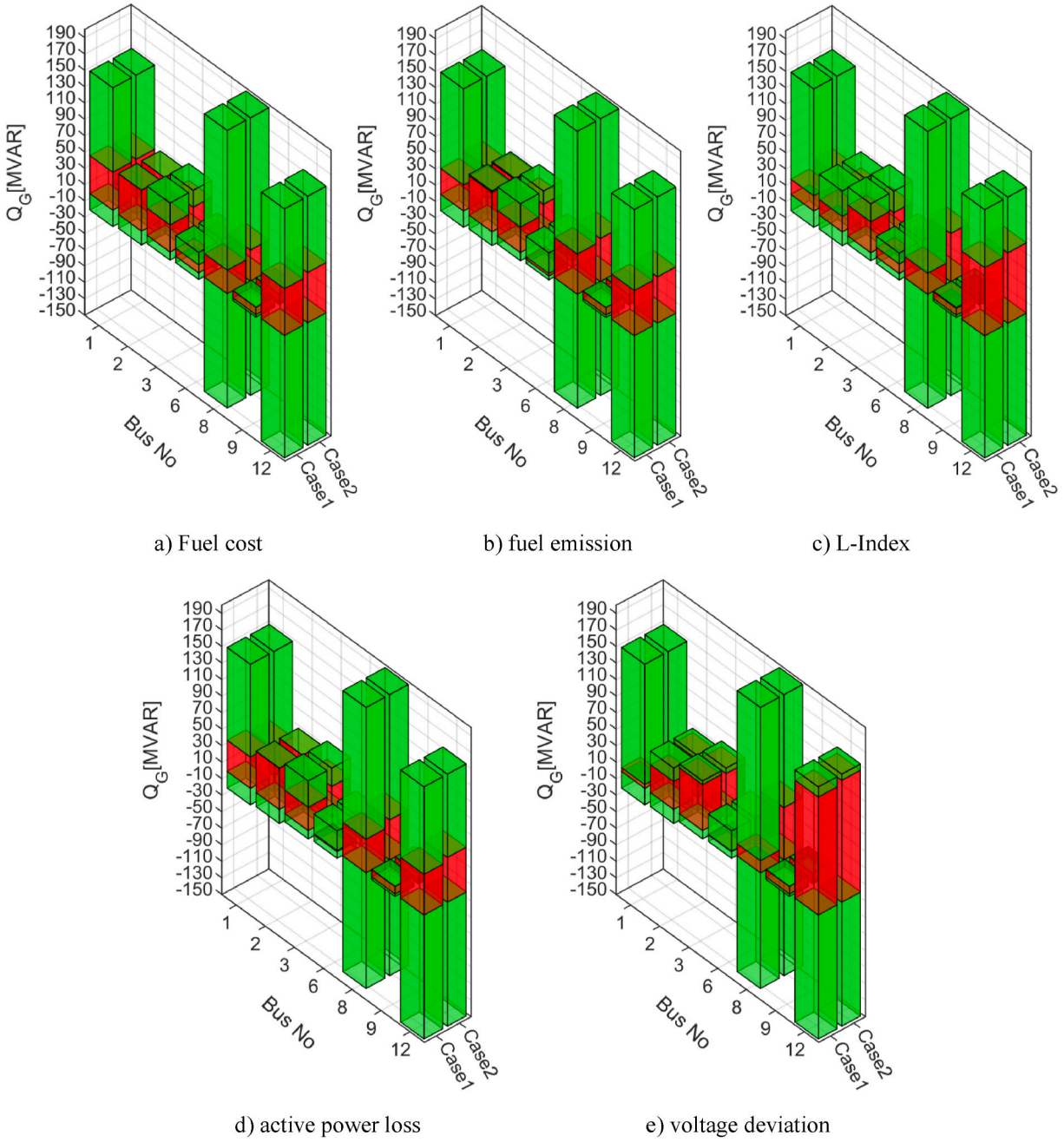

Fig. 8. Generator reactive power outputs for IEEE 57 Bus system.

problem without contravening the power system security and technical constraints. To demonstrate the effectiveness of the proposed MEBO method, common test scenarios were determined after an extensive literature survey on with wind energy and without wind energy IEEE 30-bus and IEEE 57-bus systems using the same constraint limits.

The excellent performance of MEBO is validated via a transparent comparison with state-of-the-art methodologies in the literature, where constraints are not violated. The method is capable of markedly reducing the voltage deviation function, which must never be compromised due to system constraints, to 0.0842 p.u in the 30-bus system and 0.5962 p.u in the 57-bus system. Also, by including renewable plants in the power system, it is seen that the total generation cost can be reduced significantly by using the proposed method for OPF problem. Thus, this study provides optimal solutions for OPF issues in a transparent manner, ensuring that system safety limits are not compromised. Consequently, it will contribute the comparison of new techniques proposed by researchers who adhere to system constraints.

Data availability

The data used in the manuscript are available from the cited literature. Also, the data will be made available on request.

CRediT authorship contribution statement

Kadir Abaci: Writing – review & editing, Writing – original draft, Supervision, Resources, Investigation. **Zeki Yetgin:** Writing – review & editing, Writing – original draft, Software, Formal analysis, Data curation. **Volkan Yamacli:** Writing – review & editing, Writing – original draft, Visualization, Software, Methodology, Investigation. **Hakan Isiker:** Writing – review & editing, Writing – original draft, Visualization, Methodology, Conceptualization.

Declaration of competing interest

The authors declare that they have no known competing financial interests or personal relationships that could have appeared to influence the work reported in this paper.

Acknowledgements

The authors declare that no funds, grants, or other support were received during the preparation of this manuscript.

References

[1] J. Carpentier, Contribution a l'etude du dispaching economique, Bull. Soc. Francaise Electricians 8 (1962) 431–447.
[2] H.W. Dommel, W.F. Tinney, Optimal power flow solutions, IEEE Transactions on Power Apparatus and Systems PAS- 87 (1968) 1866–1876, https://doi.org/10.1109/TPAS.1968.292150.
[3] A.A. Abou El-Ela, M.A. Abido, Optimal operation strategy for reactive power control, modelling simulation and control a general Physics matter and waves electrical and, Electronics Engineering 41 (1992) 19.
[4] R. Mota-Palomino, V.H. Quintana, Sparse reactive power scheduling by A penalty function - linear programming technique, IEEE Trans. Power Syst. 1 (1986), https://doi.org/10.1109/TPWRS.1986.4334951.
[5] R.C. Burchett, H.H. Happ, D.R. Vierath, Quadratically convergent optimal power flow, IEEE Transactions on Power Apparatus and Systems PAS- 103 (1984) 3267–3275, https://doi.org/10.1109/TPAS.1984.318568.
[6] D.I. Sun, B. Ashley, B. Brewer, A. Hughes, W.F. Tinney, Optimal power flow by Newton approach, IEEE Transactions on Power Apparatus and Systems PAS-103 (1984) 2864–2880, https://doi.org/10.1109/TPAS.1984.318284.
[7] A.J. Santos, G.R.M. Da Costa, Optimal-power-flow solution by Newton's method applied to an augmented Lagrangian function, IEE Proc. Generat. Transm. Distrib. 142 (1995) 33–36.
[8] M. Rahli, P. Pirotte, Optimal load flow using sequential unconstrained minimization technique (SUMT) method under power transmission losses minimization, Elec. Power Syst. Res. 52 (1999), https://doi.org/10.1016/S0378-7796(99)00008-5.
[9] X. Yan, V.H. Quintana, Improving an interior-point-based off by dynamic adjustments of step sizes and tolerances, IEEE Trans. Power Syst. 14 (1999), https://doi.org/10.1109/59.761902.
[10] D.C. Walters, G.B. Sheble, Genetic algorithm solution of economic dispatch with valve point loading, IEEE Trans. Power Syst. 8 (1993), https://doi.org/10.1109/59.260861.
[11] L.L. Lai, J.T. Ma, R. Yokoyama, M. Zhao, Improved genetic algorithms for optimal power flow under both normal and contingent operation States, Int. J. Electr. Power Energy Syst. 19 (1997), https://doi.org/10.1016/s0142-0615(96)00051-8.
[12] J. Yuryevich, Evolutionary programming based optimal power flow algorithm, IEEE Trans. Power Syst. 14 (1999), https://doi.org/10.1109/59.801880.
[13] A.G. Bakirtzis, P.N. Biskas, C.E. Zoumas, V. Petridis, Optimal power flow by enhanced genetic algorithm, IEEE Trans. Power Syst. 17 (2002), https://doi.org/10.1109/TPWRS.2002.1007886.
[14] A. Saini, D.K. Chaturvedi, A.K. Saxena, Optimal power flow solution: a GA-fuzzy system approach, Int. J. Emerg. Elec. Power Syst. 5 (2006), https://doi.org/10.2202/1553-779X.1091.
[15] M.S. Kumari, S. Maheswarapu, Enhanced genetic algorithm based computation technique for multi-objective optimal power flow solution, Int. J. Electr. Power Energy Syst. 32 (2010), https://doi.org/10.1016/j.ijepes.2010.01.010.
[16] W. Ongsakul, T. Tantimaporn, Optimal power flow by improved evolutionary programming, Elec. Power Compon. Syst. 34 (2006), https://doi.org/10.1080/15325000691001458.
[17] A.A. Abou El Ela, M.A. Abido, S.R. Spea, Optimal power flow using differential evolution algorithm, Elec. Power Syst. Res. 80 (2010), https://doi.org/10.1016/j.epsr.2009.12.018.
[18] C. Thitithamrongchai, B. Eua-arporn, Self-adaptive differential evolution based optimal power flow for units with non-smooth fuel cost functions, Journal of Electrical Systems 3 (2007).
[19] S. Sayah, K. Zehar, Modified differential evolution algorithm for optimal power flow with non-smooth cost functions, Energy Convers. Manag. 49 (2008), https://doi.org/10.1016/j.enconman.2008.06.014.
[20] C. Li, H. Zhao, T. Chen, The hybrid differential evolution algorithm for optimal power flow based on simulated annealing and tabu search, in: 2010 International Conference on Management and Service Science, 2010, https://doi.org/10.1109/ICMSS.2010.5578512. MASS 2010.
[21] S. Li, W. Gong, C. Hu, X. Yan, L. Wang, Q. Gu, Adaptive constraint differential evolution for optimal power flow, Energy 235 (2021), https://doi.org/10.1016/j.energy.2021.121362.
[22] P.P. Biswas, P.N. Suganthan, R. Mallipeddi, G.A.J. Amaratunga, Optimal power flow solutions using differential evolution algorithm integrated with effective constraint handling techniques, Eng. Appl. Artif. Intell. 68 (2018), https://doi.org/10.1016/j.engappai.2017.10.019.
[23] M.A. Abido, Optimal power flow using particle swarm optimization, Int. J. Electr. Power Energy Syst. 24 (2002), https://doi.org/10.1016/S0142-0615(01)00067-9.
[24] D. Ben Attous, Y. Labb, Particle swarm optimisation based optimal power flow for units with non-smooth fuel cost functions, Modelling, Measurement and Control A 83 (2010).
[25] T. Niknam, M.R. Narimani, J. Aghaei, R. Azizipanah-Abarghooee, Improved particle swarm optimisation for multi-objective optimal power flow considering the cost, loss, emission and voltage stability index, IET Gener., Transm. Distrib. 6 (2012), https://doi.org/10.1049/iet-gtd.2011.0851.
[26] K. Vaisakh, L.R. Srinivas, K. Meah, Genetic evolving ant direction particle swarm optimization algorithm for optimal power flow with non-smooth cost functions and statistical analysis, Applied Soft Computing Journal 13 (2013), https://doi.org/10.1016/j.asoc.2013.07.002.

[27] L.D. Le, J. Polprasert, W. Ongsakul, D.N. Vo, D.A. Le, Stochastic weight trade-off particle swarm optimization for optimal power flow, Journal of Automation and Control Engineering 2 (2014), https://doi.org/10.12720/joace.2.1.31-37.

[28] V. Roberge, M. Tarbouchi, F. Okou, Optimal power flow based on parallel metaheuristics for graphics processing units, Elec. Power Syst. Res. 140 (2016), https://doi.org/10.1016/j.epsr.2016.06.006.

[29] E. Naderi, M. Pourakbari-Kasmaei, F.V. Cerna, M. Lehtonen, A novel hybrid self-adaptive heuristic algorithm to handle single- and multi-objective optimal power flow problems, Int. J. Electr. Power Energy Syst. 125 (2021), https://doi.org/10.1016/j.ijepes.2020.106492.

[30] A. Bhattacharya, P.K. Chattopadhyay, Application of biogeography-based optimisation to solve different optimal power flow problems, IET Gener., Transm. Distrib. 5 (2011), https://doi.org/10.1049/iet-gtd.2010.0237.

[31] P.K. Roy, D. Mandal, Quasi-oppositional biogeography-based optimization for multi-objective optimal power flow, Elec. Power Compon. Syst. 40 (2011), https://doi.org/10.1080/15325008.2011.629337.

[32] A. Ramesh Kumar, L. Premalatha, Optimal power flow for a deregulated power system using adaptive real coded biogeography-based optimization, Int. J. Electr. Power Energy Syst. 73 (2015), https://doi.org/10.1016/j.ijepes.2015.05.011.

[33] S. Duman, U. Güvenç, Y. Sönmez, N. Yörükeren, Optimal power flow using gravitational search algorithm, Energy Convers. Manag. 59 (2012), https://doi.org/10.1016/j.enconman.2012.02.024.

[34] A.R. Bhowmik, A.K. Chakraborty, Solution of optimal power flow using nondominated sorting multi objective gravitational search algorithm, Int. J. Electr. Power Energy Syst. 62 (2014), https://doi.org/10.1016/j.ijepes.2014.04.053.

[35] A.R. Bhowmik, A.K. Chakraborty, Solution of optimal power flow using non dominated sorting multi objective opposition based gravitational search algorithm, Int. J. Electr. Power Energy Syst. 64 (2015), https://doi.org/10.1016/j.ijepes.2014.09.015.

[36] S. Sivasubramani, K.S. Swarup, Multi-objective harmony search algorithm for optimal power flow problem, Int. J. Electr. Power Energy Syst. 33 (2011), https://doi.org/10.1016/j.ijepes.2010.12.031.

[37] N. Sinsuphan, U. Leeton, T. Kulworawanichpong, Optimal power flow solution using improved harmony search method, Applied Soft Computing Journal 13 (2013), https://doi.org/10.1016/j.asoc.2013.01.024.

[38] R. Arul, G. Ravi, S. Velusami, Solving optimal power flow problems using chaotic self-adaptive differential harmony search algorithm, Elec. Power Compon. Syst. 41 (2013), https://doi.org/10.1080/15325008.2013.769033.

[39] D. Karaboga, An Idea Based on Honey Bee Swarm for Numerical Optimization, Erciyes University, 2005. Technical Report TR06.

[40] M. Rezaei Adaryani, A. Karami, Artificial bee colony algorithm for solving multi-objective optimal power flow problem, Int. J. Electr. Power Energy Syst. 53 (2013), https://doi.org/10.1016/j.ijepes.2013.04.021.

[41] X. He, W. Wang, J. Jiang, L. Xu, An improved artificial bee colony algorithm and its application to multi-objective optimal power flow, Energies 8 (2015), https://doi.org/10.3390/en8042412.

[42] H.R.E.H. Bouchekara, M.A. Abido, M. Boucherma, Optimal power flow using Teaching-Learning-Based Optimization technique, Elec. Power Syst. Res. 114 (2014), https://doi.org/10.1016/j.epsr.2014.03.032.

[43] S. Ermiş, Multi-objective optimal power flow using a modified weighted teaching-learning based optimization algorithm, Elec. Power Compon. Syst. 51 (2023), https://doi.org/10.1080/15325008.2023.2239237.

[44] M. Ghasemi, S. Ghavidel, M. Gitizadeh, E. Akbari, An improved teaching-learning-based optimization algorithm using Lévy mutation strategy for non-smooth optimal power flow, Int. J. Electr. Power Energy Syst. 65 (2015), https://doi.org/10.1016/j.ijepes.2014.10.027.

[45] A. Panda, M. Tripathy, Optimal power flow solution of wind integrated power system using modified bacteria foraging algorithm, Int. J. Electr. Power Energy Syst. 54 (2014), https://doi.org/10.1016/j.ijepes.2013.07.018.

[46] M. Ghasemi, S. Ghavidel, M.M. Ghanbarian, M. Gharibzadeh, A. Azizi Vahed, Multi-objective optimal power flow considering the cost, emission, voltage deviation and power losses using multi-objective modified imperialist competitive algorithm, Energy 78 (2014), https://doi.org/10.1016/j.energy.2014.10.007.

[47] A.A. El-Fergany, H.M. Hasanien, Single and multi-objective optimal power flow using grey wolf optimizer and differential evolution algorithms, Elec. Power Compon. Syst. 43 (2015), https://doi.org/10.1080/15325008.2015.1041625.

[48] A. Meng, C. Zeng, P. Wang, D. Chen, T. Zhou, X. Zheng, H. Yin, A high-performance crisscross search based grey wolf optimizer for solving optimal power flow problem, Energy 225 (2021), https://doi.org/10.1016/j.energy.2021.120211.

[49] M. Ahmad, N. Javaid, I.A. Niaz, A. Almogren, A. Radwan, A bio-inspired heuristic algorithm for solving optimal power flow problem in hybrid power system, IEEE Access 9 (2021), https://doi.org/10.1109/ACCESS.2021.3131161.

[50] A.A.A. Mohamed, Y.S. Mohamed, A.A.M. El-Gaafary, A.M. Hemeida, Optimal power flow using moth swarm algorithm, Elec. Power Syst. Res. 142 (2017), https://doi.org/10.1016/j.epsr.2016.09.025.

[51] K. Abaci, V. Yamacli, Differential search algorithm for solving multi-objective optimal power flow problem, Int. J. Electr. Power Energy Syst. 79 (2016), https://doi.org/10.1016/j.ijepes.2015.12.021.

[52] A.E. Chaib, H.R.E.H. Bouchekara, R. Mehasni, M.A. Abido, Optimal power flow with emission and non-smooth cost functions using backtracking search optimization algorithm, Int. J. Electr. Power Energy Syst. 81 (2016), https://doi.org/10.1016/j.ijepes.2016.02.004.

[53] S. Duman, Symbiotic organisms search algorithm for optimal power flow problem based on valve-point effect and prohibited zones, Neural Comput. Appl. 28 (2017), https://doi.org/10.1007/s00521-016-2265-0.

[54] H. Pulluri, R. Naresh, V. Sharma, A solution network based on stud krill herd algorithm for optimal power flow problems, Soft Comput. 22 (2018), https://doi.org/10.1007/s00500-016-2319-3.

[55] A. Mukherjee, V. Mukherjee, Solution of optimal power flow with FACTS devices using a novel oppositional krill herd algorithm, Int. J. Electr. Power Energy Syst. 78 (2016), https://doi.org/10.1016/j.ijepes.2015.12.001.

[56] A. Saha, P. Das, A.K. Chakraborty, Water evaporation algorithm: a new metaheuristic algorithm towards the solution of optimal power flow, Engineering Science and Technology, an International Journal 20 (2017), https://doi.org/10.1016/j.jestch.2017.12.009.

[57] H. Buch, I.N. Trivedi, P. Jangir, Moth flame optimization to solve optimal power flow with non-parametric statistical evaluation validation, Cogent Eng 4 (2017), https://doi.org/10.1080/23311916.2017.1286731.

[58] M.A. Taher, S. Kamel, F. Jurado, M. Ebeed, An improved moth-flame optimization algorithm for solving optimal power flow problem, International Transactions on Electrical Energy Systems 29 (2019), https://doi.org/10.1002/etep.2743.

[59] W. Warid, H. Hizam, N. Mariun, N.I. Abdul-Wahab, Optimal power flow using the Jaya algorithm, Energies 9 (2016), https://doi.org/10.3390/en9090678.

[60] W. Warid, Optimal power flow using the AMTPG-Jaya algorithm, Applied Soft Computing Journal 91 (2020), https://doi.org/10.1016/j.asoc.2020.106252.

[61] A.F. Attia, R.A. El Sehiemy, H.M. Hasanien, Optimal power flow solution in power systems using a novel Sine-Cosine algorithm, Int. J. Electr. Power Energy Syst. 99 (2018), https://doi.org/10.1016/j.ijepes.2018.01.024.

[62] A.M. Shaheen, R.A. El-Sehiemy, H.M. Hasanien, A. Ginidi, An enhanced optimizer of social network search for multi-dimension optimal power flow in electrical power grids, Int. J. Electr. Power Energy Syst. 155 (2024) 109572, https://doi.org/10.1016/j.ijepes.2023.109572.

[63] N. Guha, Z. Wang, M. Wytock, A. Majumdar, Machine Learning for AC Optimal Power Flow, 2019.

[64] J. Rahman, C. Feng, J. Zhang, A learning-augmented approach for AC optimal power flow, Int. J. Electr. Power Energy Syst. 130 (2021), https://doi.org/10.1016/j.ijepes.2021.106908.

[65] A.M. Shaheen, R.A. El-Sehiemy, E.E. Elattar, A.S. Abd-Elrazek, A modified crow search optimizer for solving non-linear OPF problem with emissions, IEEE Access 9 (2021), https://doi.org/10.1109/ACCESS.2021.3060710.

[66] S. Abd el-sattar, S. Kamel, M. Ebeed, F. Jurado, An improved version of salp swarm algorithm for solving optimal power flow problem, Soft Comput. 25 (2021), https://doi.org/10.1007/s00500-020-05431-4.

[67] J.H. Zhu, J.S. Wang, X.Y. Zhang, H.M. Song, Z.H. Zhang, Mathematical distribution coyote optimization algorithm with crossover operator to solve optimal power flow problem of power system, Alex. Eng. J. 69 (2023), https://doi.org/10.1016/j.aej.2023.02.023.

[68] H. Su, Q. Niu, Z. Yang, Optimal power flow using improved cross-entropy method, Energies 16 (2023), https://doi.org/10.3390/en16145466.
[69] M. Ahmad, N. Javaid, I.A. Niaz, I. Ahmed, M.A. Hashmi, An orthogonal learning bird swarm algorithm for optimal power flow problems, IEEE Access 11 (2023), https://doi.org/10.1109/ACCESS.2023.3253796.
[70] M. Premkumar, C. Kumar, T. Dharma Raj, S.D.T. Sundarsingh Jebaseelan, P. Jangir, H. Haes Alhelou, A reliable optimization framework using ensembled successive history adaptive differential evolutionary algorithm for optimal power flow problems, IET Gener., Transm. Distrib. 17 (2023) 1333–1357, https://doi.org/10.1049/gtd2.12738.
[71] W. Yi, Z. Lin, Y. Lin, S. Xiong, Z. Yu, Y. Chen, Solving optimal power flow problem via improved constrained adaptive differential evolution, Mathematics 11 (2023), https://doi.org/10.3390/math11051250.
[72] M. Kaur, N. Narang, Optimal power flow solution using space transformational invasive weed optimization algorithm, Iranian Journal of Science and Technology - Transactions of Electrical Engineering (2023), https://doi.org/10.1007/s40998-023-00592-y.
[73] A.M. Shaheen, R.A. El-Sehiemy, M.M. Alharthi, S.S.M. Ghoneim, A.R. Ginidi, Multi-objective jellyfish search optimizer for efficient power system operation based on multi-dimensional OPF framework, Energy 237 (2021), https://doi.org/10.1016/j.energy.2021.121478.
[74] O. Akdag, A. Ates, C. Yeroglu, Modification of Harris hawks optimization algorithm with random distribution functions for optimum power flow problem, Neural Comput. Appl. 33 (2021), https://doi.org/10.1007/s00521-020-05073-5.
[75] O. Akdag, A improved Archimedes optimization algorithm for multi/single-objective optimal power flow, Elec. Power Syst. Res. 206 (2022), https://doi.org/10.1016/j.epsr.2022.107796.
[76] V. Bathina, R. Devarapalli, F.P. García Márquez, Hybrid approach with combining cuckoo-search and grey-wolf optimizer for solving optimal power flow problems, Journal of Electrical Engineering and Technology 18 (2023), https://doi.org/10.1007/s42835-022-01301-1.
[77] R. Keswani, H.K. Verma, S.K. Sharma, Multi-objective optimal power flow employing a hybrid sine cosine–grey wolf optimizer, Iranian Journal of Science and Technology - Transactions of Electrical Engineering (2023), https://doi.org/10.1007/s40998-023-00631-8.
[78] M. Ahmadipour, M. Murtadha Othman, R. Bo, M. Sadegh Javadi, H. Mohammed Ridha, M. Alrifaey, Optimal power flow using a hybridization algorithm of arithmetic optimization and aquila optimizer, Expert Syst. Appl. 235 (2024) 121212, https://doi.org/10.1016/j.eswa.2023.121212.
[79] S.S. Reddy, Optimal power flow using hybrid differential evolution and harmony search algorithm, International Journal of Machine Learning and Cybernetics 10 (2019), https://doi.org/10.1007/s13042-018-0786-9.
[80] T.T. Nguyen, A high performance social spider optimization algorithm for optimal power flow solution with single objective optimization, Energy 171 (2019), https://doi.org/10.1016/j.energy.2019.01.021.
[81] M. Ebeed, M.A. Abdelmotaleb, N.H. Khan, R. Jamal, S. Kamel, A.G. Hussien, H.M. Zawbaa, F. Jurado, K. Sayed, A Modified Artificial Hummingbird Algorithm for solving optimal power flow problem in power systems, Energy Rep. 11 (2024) 982–1005, https://doi.org/10.1016/J.EGYR.2023.12.053.
[82] S.P. Dash, K.R. Subhashini, P. Chinta, Development of a Boundary Assigned Animal Migration Optimization algorithm and its application to optimal power flow study, Expert Syst. Appl. 200 (2022), https://doi.org/10.1016/j.eswa.2022.116776.
[83] P.P. Biswas, P.N. Suganthan, G.A.J. Amaratunga, Optimal power flow solutions incorporating stochastic wind and solar power, Energy Convers. Manag. 148 (2017) 1194–1207, https://doi.org/10.1016/J.ENCONMAN.2017.06.071.
[84] R. Roy, H.T. Jadhav, Optimal power flow solution of power system incorporating stochastic wind power using Gbest guided artificial bee colony algorithm, Int. J. Electr. Power Energy Syst. 64 (2015), https://doi.org/10.1016/j.ijepes.2014.07.010.
[85] L. Shi, C. Wang, L. Yao, Y. Ni, M. Bazargan, Optimal power flow solution incorporating wind power, IEEE Syst. J. 6 (2012) 233–241, https://doi.org/10.1109/JSYST.2011.2162896.
[86] M.D. Raj, N.B. Muthuselvan, P. Somasundaram, Swarm-inspired artificial bee colony algorithm for solving optimal power flow with wind farm, Arabian J. Sci. Eng. 39 (2014), https://doi.org/10.1007/s13369-014-1084-9.
[87] A. Man-Im, W. Ongsakul, J.G. Singh, M.N. Madhu, Multi-objective optimal power flow considering wind power cost functions using enhanced PSO with chaotic mutation and stochastic weights, Electr. Eng. 101 (2019), https://doi.org/10.1007/s00202-019-00815-8.
[88] E. Kaymaz, S. Duman, U. Guvenc, Optimal power flow solution with stochastic wind power using the Lévy coyote optimization algorithm, Neural Comput. Appl. 33 (2021), https://doi.org/10.1007/s00521-020-05455-9.
[89] V. Yadav, S.P. Ghoshal, Optimal power flow for IEEE 30 and 118-bus systems using Monarch Butterfly optimization, in: International Conference on Technologies for Smart City Energy Security and Power: Smart Solutions for Smart Cities, ICSESP 2018 - Proceedings, 2018, https://doi.org/10.1109/ICSESP.2018.8376670.
[90] A. Kumar, R.K. Misra, D. Singh, Improving the local search capability of effective butterfly optimizer using covariance matrix adapted retreat phase, in: 2017 IEEE Congress on Evolutionary Computation, CEC 2017 - Proceedings, 2017, https://doi.org/10.1109/CEC.2017.7969524.
[91] I. Kumarswamy, P. Ramanareddy, Analysis of voltage stability using L-index method, Int. J. Electr. Eng. 4 (2011) 483–498.
[92] A. Kumar, R.K. Misra, D. Singh, Butterfly optimizer, in: 2015 IEEE Workshop on Computational Intelligence: Theories, Applications and Future Directions (WCI), 2015, pp. 1–6, https://doi.org/10.1109/WCI.2015.7495523.
[93] D. Zaharie, A comparative analysis of crossover variants in differential evolution. Proceedings of the IMCSIT, 2007.
[94] R. Tanabe, A. Fukunaga, Success-history based parameter adaptation for Differential Evolution, in: 2013 IEEE Congress on Evolutionary Computation, CEC 2013, 2013, https://doi.org/10.1109/CEC.2013.6557555.
[95] H. Saadat, Power system analysis: third edition, systems, controls, embedded systems. Energy, and Machines 3, 2011.
[96] M. Shahidehpour, Y. Wang, C. Appendix, IEEE30 bus system data, in: Communication and Control in Electric Power Systems: Applications of Parallel and Distributed Processing, 2003, pp. 493–495, https://doi.org/10.1002/0471462926.app3.
[97] U.W. Archive, 100.0 1961 W IEEE 57 Bus Test Case, 1993. https://labs.ece.uw.edu/pstca/pf57/ieee57cdf.txt.
[98] J. Zhang, J. Cai, H. Zhang, T. Chen, NSGA-III integrating eliminating strategy and dynamic constraint relaxation mechanism to solve many-objective optimal power flow problem, Appl. Soft Comput. 146 (2023), https://doi.org/10.1016/j.asoc.2023.110612.
[99] F. Daqaq, M. Ouassaid, R. Ellaia, A new meta-heuristic programming for multi-objective optimal power flow, Electr. Eng. 103 (2021), https://doi.org/10.1007/s00202-020-01173-6.
[100] H.R.E.H. Bouchekara, A.E. Chaib, M.A. Abido, R.A. El-Sehiemy, Optimal power flow using an improved colliding bodies optimization algorithm, Applied Soft Computing Journal 42 (2016), https://doi.org/10.1016/j.asoc.2016.01.041.
[101] P. Pravina, M.R. Babu, A.R. Kumar, Solving optimal power flow problems using adaptive quasi-oppositional differential migrated biogeography-based optimization, Journal of Electrical Engineering and Technology 16 (2021), https://doi.org/10.1007/s42835-021-00739-z.
[102] A.A. El-Fergany, H.M. Hasanien, Tree-seed algorithm for solving optimal power flow problem in large-scale power systems incorporating validations and comparisons, Applied Soft Computing Journal 64 (2018), https://doi.org/10.1016/j.asoc.2017.12.026.
[103] A.M. Shaheen, S.M. Farrag, R.A. El-Sehiemy, MOPF solution methodology, IET Gener., Transm. Distrib. 11 (2017), https://doi.org/10.1049/iet-gtd.2016.1379.
[104] M. Amroune, Wind integrated optimal power flow considering power losses, voltage deviation, and emission using equilibrium optimization algorithm, Energy Ecol Environ 7 (2022), https://doi.org/10.1007/s40974-022-00249-2.
[105] A. Ali, A. Hassan, M.U. Keerio, N.H. Mugheri, G. Abbas, M. Hatatah, E. Touti, A. Yousef, A novel solution to optimal power flow problems using composite differential evolution integrating effective constrained handling techniques, Sci. Rep. 14 (2024) 6187, https://doi.org/10.1038/s41598-024-56590-5.
[106] A. Alhejji, M. Ebeed Hussein, S. Kamel, S. Alyami, Optimal power flow solution with an embedded center-node unified power flow controller using an adaptive grasshopper optimization algorithm, IEEE Access 8 (2020), https://doi.org/10.1109/ACCESS.2020.2993762.
[107] M.Z. Islam, M.L. Othman, N.I.A. Wahab, V. Veerasamy, S.R. Opu, A. Inbamani, V. Annamalai, Marine predators algorithm for solving single-objective optimal power flow, PLoS One 16 (2021), https://doi.org/10.1371/journal.pone.0256050.
[108] H.R.E.H. Bouchekara, Optimal power flow using black-hole-based optimization approach, Applied Soft Computing Journal 24 (2014), https://doi.org/10.1016/j.asoc.2014.08.056.

[109] R.V. Rao, V.J. Savsani, J. Balic, Teaching-learning-based optimization algorithm for unconstrained and constrained real-parameter optimization problems, Eng. Optim. 44 (2012), https://doi.org/10.1080/0305215X.2011.652103.
[110] H. Pulluri, R. Naresh, V. Sharma, An enhanced self-adaptive differential evolution based solution methodology for multiobjective optimal power flow, Applied Soft Computing Journal 54 (2017), https://doi.org/10.1016/j.asoc.2017.01.030.
[111] E.E. Elattar, A.M. Shaheen, A.M. Elsayed, R.A. El-Sehiemy, Optimal power flow with emerged technologies of voltage source converter stations in meshed power systems, IEEE Access 8 (2020), https://doi.org/10.1109/ACCESS.2020.3022919.
[112] Y. Tian, Z. Shi, Y. Zhang, L. Zhang, H. Zhang, X. Zhang, Solving optimal power flow problems via a constrained many-objective co-evolutionary algorithm, Front. Energy Res. 11 (2023), https://doi.org/10.3389/fenrg.2023.1293193.
[113] R.D. Zimmerman, C.E. Murillo-Sánchez, MATPOWER (2020), https://doi.org/10.5281/zenodo.4074135.